UM Report #025921-13-T

THE UNIVERSITY OF MICHIGAN

COLLEGE OF ENGINEERING

DEPARTMENT OF ELECTRICAL ENGINEERING & COMPUTER SCIENCE

Radiation Laboratory

SEMI-ANNUAL REPORT ON NASA GRANT NAG-2-541

Period: February 1990 - September 1990

Radiation Laboratory
Department of Electrical Engineering
and Computer Science
The University of Michigan
Ann Arbor, MI 48109

National Aeronautics and
Space Administration
Ames Research Center
Moffett Field, CA 94035
Grant NAG-2-541

Ann Arbor, Michigan

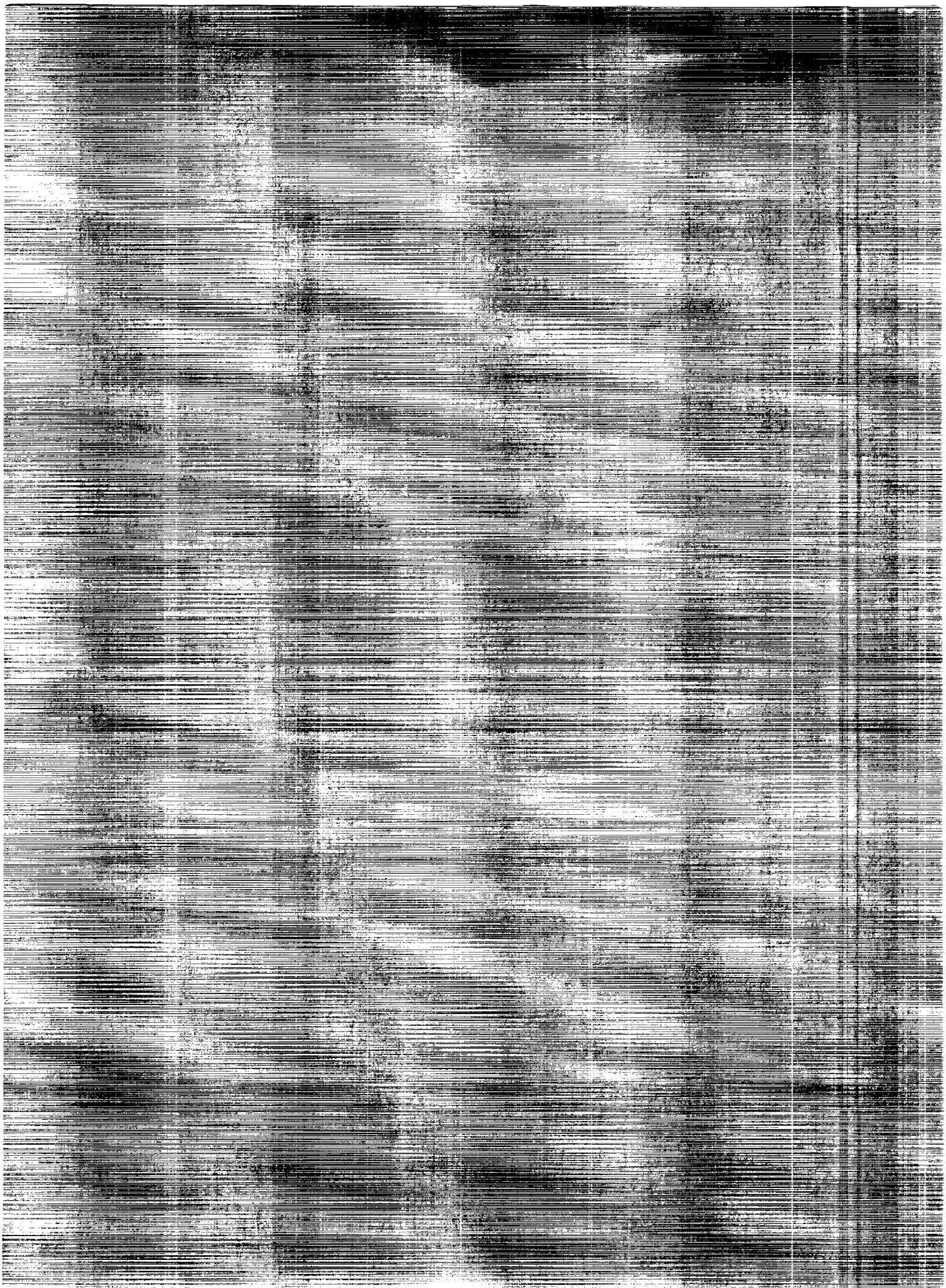

SEMI-ANNUAL REPORT

FOR

NASA Grant NAG-2-541

NASA Technical Monitor: Alex Woo

Institution: The Radiation Laboratory
Department of Electrical Engineering
and Computer Science
The University of Michigan
Ann Arbor, MI 48109-2122

Period Covered: February 1990 - September 1990

Report Title: Semi-Annual Report

Principal Investigator: John L. Volakis
Telephone: (313) 764-0500

Preface

This semi-annual report describes our progress during the period from February 1990 to September 1990. Several technical reports and papers have been written and these are listed at the end of each task.

There are two tasks described in this report. Each should be read independently. That is, figure and reference numbering is consecutive only within the description of the task. As can be expected, the progress reports are very brief and the reader should refer to the referenced technical reports for detailed coverage. A total of sixteen technical reports have already been submitted and two more are currently being prepared. Also, more than 18 publications to refereed journals and more than 17 conference papers have resulted from this sponsored research.

TABLE OF CONTENTS

		Page #
	PREFACE	i
TASK:	A FINITE ELEMENT CONJUGATE GRADIENT FFT METHOD FOR SCATTERING	
	Abstract	1
	Objective	1
	Progress	3
	Pre- and Post-Processing Algorithms	3
	3D Algorithms for Bodies of Revolution	5
	Conclusions	6
	Transitions	6
	References	7
	Publications Resulting from this Research	10
TASK:	ANALYTICAL SOLUTIONS WITH GENERALIZED IMPEDANCE BOUNDARY CONDITIONS (GIBC)	
	Abstract	13
	Objective	13
	Introduction	13
	Dual Integral Equation Formulation	15
	Solution of the Diffracted Field	20
	Diffraction by Thin Single Layer Discontinuous Strips	22
	Modal Decomposition of the Symmetric Slab Fields	25
	Exterior Cross Section Functions	28
	Interior Cross Section Functions	29
	Recasting of the Dual Integral Equation Solution for a Material Junction	31

Determination of the Constants 34

Validation of the Solution 37

Other Applications of the GIBC/GSTC 37

Appendix 39

References 41

Publications Resulting from this Research 44

p 24

Task Title: A Finite Element Conjugate Gradient FFT Method for Scattering

Investigators: Jeffery D. Collins, John Zapp, Chang-Yu Hsa and John L. Volakis

Period Covered: February 1990 - September 1990

ABSTRACT

An extension of the two-dimensional formulation developed last year is presented for a three dimensional body of revolution. With the introduction of a Fourier expansion of the vector electric and magnetic fields, a coupled two-dimenional system is generated and solved via the finite-element method. As before, an exact boundary condition is employed to terminate the mesh and the FFT is used to evaluate the boundary integrals for low O(n) memory demand when an iterative solution algorithm is used. Again, by virtue of the finite element method the algorithm is applicable to structures of arbitrary material composition.

Several improvements to our two-dimensional algorithm are also described. These include (1) modifications for terminating the mesh at circular boundaries without distorting the convolutionality of the boundary integrals, (2) the development of our own non-proprietery mesh generation routines for two-dimensional applications, (3) the development of preprocessors for interfacing SDRC IDEAS@ with the main algorithm, and (4) the development of post-processing algorithms based on the public domain package GRAFIC to generate 2D and 3D gray level and color field maps.

OBJECTIVE

The objective of this task is to develop innovative techniques and related software for scattering by three dimensional composite structures. The proposed analysis is a hybrid finite element-boundary integral method formulated to have an O(n) memory demand. This low storage is achieved by employing the FFT to evaluate all boundary integrals and resorting to an iterative solution algorithm. Particular emphasis in this task is the generation of software applicable to airborne vehicles and the validation of these by comparison with measured and other reference data. Because the approach is new, a step by step development procedure has been proposed over a three-year period. During the first year the technique was developed and implemented for two-dimensional composite structures. Support software for the two-dimenional analysis such as pre- and post-processor routines were developed during the second year and a formulation was also developed and implemented for three-dimensional bodies of revolution. Finally, during the third year, we will develop, implement, and test the method for arbitrary three dimensional structures.

BACKGROUND

Interest in three-dimensional (3-D) methods has increased in recent years, however, the associated demands in computation time and storage are often prohibitive for electrically large 3-D bodies. Vector and concurrent (i.e. hypercube, connection, etc.) computers are beginning to alleviate the first of these demands, but a minimization of the storage requirements is essential for treating large structures.

The traditional Conjugate Gradient Fast Fourier Transform (CGFFT) method [1]-[4] is one such frequency domain solution approach which requires O(n) storage for the solution of n equations. This method involves the use of FFTs whose dimension equals that of the structure under consideration [5]-[7] and, therefore, demands excessive computation time when used in an iterative algorithm. Also, the standard CGFFT requires uniform rectangular gridding that unnecessarily includes the impenetrable portions of the scatterer. With these issues in mind, a new solution approach is propsed for solving scattering problems. The proposed method will be referred to as the Finite Element-Conjugate Gradient Fast Fourier Transform (FE-CGFFT) method.

During last year's effort the FE-CGFFT method was developed for two-dimensional scatterers where the finite element mesh was terminated at a rectangular box. Inside the box boundaries, Helmholtz equation is solved via the finite element method and the boundary constraint is obtained by an appropriate integral equation which implicitly satisfies the radiation condition. Along the parallel sides of the box, this integral becomes a convolution and is, therefore, amenable to evaluation via the FFT. The dimension of the required FFT in this hybrid method is one less than the dimensionality of the structure thus, making it attractive for 3-D simulations. Also, because it incorporates the finite element method, the FE-CGFFT formulation remains valid regardless of the structure's geometry and material composition.

The proposed method described in the University of Michigan Report 025921-6-T (see also [8]) is similar to the moment method version developed by Jin [9]. Jin's method was in turn based on work published in the early 70's by McDonald and Wexler [10] who introduced an approach to solve unbounded field problems. The proposed method is also similar to other methods (a few of which will be mentioned here), neither of which provides a storage reduction comparable to the proposed FE-CGFFT method. The unimoment method [11] uses finite elements inside a fictitious circular boundary and an eigenfunction expansion to represent the field in the external region. The coefficients of the expansion are then determined by enforcing field continuity at the finite element (FE) mesh boundary. The coupled finite element-boundary element method [12] uses the finite

element method within the boundary and the boundary element method to provide the additional constraint at the termination of the mesh. Unlike the proposed method, the solution in [12] was accomplished by direct matrix inversion (as in [9]), and the outer mesh boundary is not rectangular to take advantage of the FFT for the evaluation of the boundary integrals.

PROGRESS

The proposed FE-CGFFT formulation was implemented last year (see Figs. 1 and 2) but as can be expected, the rectangular mesh boundary does not always lead to the most efficient formulation, particularly when dealing with structures whose outer boundary is not rectangular. Because of this, during this year we developed and implemented a formulation which permits mesh termination at circular (see Fig. 3) boundaries for the 2D case with the corresponding boundary enclosure being a pillbox for the 3D case (see Fig. 4). As before, these boundaries lead to convolutional integrals and do not therefore destroy the O(n) memory demand of the method. The FE-CGFFT formulation relating to circular (and ogival) boundary enclosures is described in the University of Michigan report 025921-11-T (see also [13]) and results based on its implementation are shown in Figures 5 and 6. Fig. 5 shows bistatic scattering patterns for a coated circular cylinder with a conductor radius of 3λ, 0.05λ coating thickness and material properties $\varepsilon_r = 3\text{-}j5$ and $\mu_r = 1.5 - j0.5$. The agreement with the series solution result is excellent. In Fig. 6 a backscatter pattern is shown for a $\lambda/2 \times 1\lambda$ conducting ogive (see Fig. 3). In comparison with the moment method results, the agreement is again excellent. Additional results are given in Figure 7 for a missle-like shape scatterer.

Pre- and Post-Processing Algorithms

The availability of pre- and post-processing algorithms is crucial for the generation of the geometry and display of results in a graphical form. Generally, it is desirable that these tasks be done with a graphical user interface (GUI) and possibly in an X-window setting. Part of this year's effort was therefore devoted to the development of such algorithms and/or interfaces for the more sophisticated commercial pre- and post-processing packages.

For the most part, there exist commercial geometry, mesh generation and post-processing packages which are highly interactive and graphical. Nevertheless, there is always a need for a suitable interface or data interpretor between the commercial packages and the solution algorithm described in the previous section. The specific package interfaced with the computational algorithm was SDRC IDEAS@ and the selection of this was based on its availability on the U-M Network, its versatility, graphical user interface, and capability to generate meshes for 2D and 3D structures. Furthermore, a new version of SDRC IDEAS@, to be released soon, will support X-windows. IDEAS was developed for mechanical design purposes, but its geometry and finite element mesh generation modules are particularly suited for our needs. The geometry is defined graphically using the area (for 2D) or solids (for 3D) modeling capability provided by the module Geomod. Alternatively, the user may choose to enter the geometry in terms of individual points, surve segments (for 2D) or surfaces (for 3D). Once the geometry is entered, mesh areas or regions are specified and either a mapped mesh or free mesh can be generated. Further, individual nodes and/or elements may be inputted as desired using the CREATE command. Once the mesh is generated, two files are created, one containing the nodes and their corresponding coordinates, and another specifying the nodes of each element. These files are then read by an interpretor which creates a new input file compatible with the format required by the computational modules.

Examples of two-dimensional meshes generated with SDRC IDEAS@ were shown in Figures 1, 2b and 7, and these are in a form suitable for the FE-CGFFT analysis. Some three-dimensional meshes are also displayed in Figure 8 for an ogive and missile-like structures. As seen, the 3D meshes are terminated at a cylindrical surface, tightly enclosing the scatterer which is the intended enclosure for the proposed FE-CGFFT method. A brief manual for geometry and mesh generation using SDRC IDEAS@ is currently being prepared.

SDRC IDEAS@ is a rather sophisticated package and its use is certainly preferable for 3D modeling and mesh generation. For 2D mesh generation, though, it is possible to construct a non-proprietory package without much effort, and which is also simpler without a serious sacrifice in versatility. Clearly, the primary reason for resorting to such an algorithm is to permit mesh generation at sites not having a license for SDRC IDEAS@. The specific geometry and mesh generation package developed for this purpose is based on the algorithm described in [14]. Examples of free meshes generated by this package are displayed in Figures 2a and 3. The package is interactive/menu driven and can be readily used without much preparation. The mesh can be displayed in the Apollo screens or a postscript file may be generated for display on other workstations. At present,

visualization cannot be done in an X-window but this capability is planned for early next year.

A variety of post-processing capabilities have also been exmployed for a graphical display of the output data. The output is either in the form of echowidth plots as a function of observation and/or incidence angle or in the form of gray level field maps. Color instead of gray level field maps can also be generated at those workstations which support this feature. Generally, all echowidth plots are generated and displayed using standard software, and each workstation provides its own selection. To generate and visualize the gray level and color field maps we employed the public domain package GRAFIC. An example of a gray level plot is shown in Figure 9. This is generated from a postscript file and can thus be displayed on other sponsor machines.

3D Algorithm for Bodies of Revolution

Before extending the presented 2D formulation to scattering by arbitrary 3D structures, it is instructive that we first consider its implementation for a restrictive class of 3D bodies. In particular, during this year an algorithm was developed for scattering by inhomogeneous bodies of revolution. Because of the symmetry of this structure, it is only necessary to discretize it in a single plane slicing the structure as shown in Figure 10. A knowledge of the fields over this cross-section is then sufficient to generate the fields everywhere by employing a Fourier expansion in the azimuthal direction. Clearly, the discretization can be accomplished using a 2D mesh generation routine and this is the primary reasons for considering this class of structures. Also, the storage requirements are comparable to that of the 2D formulation although, as expected, the computational intensity is much greater.

The mathematical details pertaining to the BOR formulation will be presented at sufficient detail in an upcoming technical report. Briefly, the method consists of the following steps

1) A Fourier expansion is used to expand the fields in terms of those over a single cross-section of the BOR.

2) The fields in the finite-element region are then formulated via the Coupled Azimuthal Potential (CAP) method as described in [15]. This results in a banded finite-element matrix in terms of the boundary fields.

3) The boundary fields are formulated via the usual Stratton-Chu equations which are then discretized via the boundary element method. As before, the boundary enclosure is chosen to yield convolutional integrals computed via the FFT.

4) The finite-element and boundary-element systems are coupled via the boundary fields and solved via the CGFFT method maintaining an O(n) storage requirement, where n is the number of nodes over a single cross section of the BOR.

Presently, a code has been written based on the proposed formulation and is in the final stages of the validation process.

CONCLUSIONS

So far, we have formulated and implemented the FE-CGFFT method for a variety of 2D structures and we are now in the process of completing its implementation for BOR structures. The method was proposed because of its versatility, accuracy and low memory demand in comparison with other methodologies, and all of these attributes have been demonstrated in the testing and validation process. It is therefore a promising method for general 3D implementations to be considered in the following year.

TRANSITIONS

The validation of the 3D BOR formulation is expected to be completed by early Fall 1990. We will then begin the development and implementation of the formulation for arbitrary 3D structures. This implementation is expected to be much more involved than those considered earlier and the same if true for the geometry and mesh generation. It is therefore, likely that the proposed 3D implementation may not be completed by the end of the 3rd year. Also, because of the need to generate suitable pre-processing and post-processing algorithms additional man-hours are required during the third year of this effort. Most likely, a practical user-oriented validated and benchmarked code will not be available until the fourth year. As part of this effort it would also be desirable to design and develop a graphical user interface (GUI) compatible with the X-window platforms. The GUI is

particularly necessary for the 3D analysis package. Otherwise, the user would be faced with a long list of subprograms whose interfacing would likely be cumbersome.

The proposed FE-CGFFT formulation employs an exact boundary condition at the termination of the mesh. This eliminates a need to extend the mesh far from the scatterer leading to a substantial savings in storage requirements. However, this storage reduction and solution accuracy is achieved at the expense of computational complexity and intensity. In many cases, though, where accuracy is not of primary concern, one could resort to the use of non-exact (i.e. absorbing boundary conditions), for terminating the mesh. This leads to completely sparse matricies which can be solved more efficiently using special purpose algorithms. In the future, it is therefore desirable to include this formulation as an option to the user. Also, a new class of boundary conditions are currently being investigated for terminating the mesh.

REFERENCES

[1] T.K. Sarkar, E. Arvas and S.M. Rao, "Application of FFT and the conjugate gradient method for the solution of electromagnetic radiation from electrically large and small conducting bodies," IEEE Trans. Antennas Propagat., Vol. AP-30, pp. 409-418, May 1986.

[2] T.J. Peters and J.L. Volakis, "Scattering from thin planar layers of arbitrary composition," IEEE Trans. Antennas Propagat., AP-36, pp. 518-526, April 1988.

[3] M.F. Cátedra, J.G. Cuevas and L. Nuño, "A scheme to analyze conducting plates of resonent size using the conjugate gradient method and the fast Fourier transform," IEEE Trans. Antennas Propagat., AP-36, pp. 1744-1752, Dec. 1988.

[4] C.Y. Shen, K.J. Gloner, M.I. Sancer and A.D. Varvatsis, "The discrete Fourier tranform method of solving differential-integral equations in scattering theory," To appear in IEEE Trans. Antennas Propagat.

[5] C.Y. Shen, "Application of the discrete Fourier transform method to thin dielectric structures," IEEE Trans. Antennas Propagat., Vol. AP-37, pp. 1277-1283, Oct. 1989.

[6] M.F. Cátedra, E. Gago, and L. Nuño, "A numerical scheme to obtain the RCS of three-dimensional bodies of resonant size using the conjugate gradient method and the fast Fourier transform," IEEE Trans. Antennas Propagat., AP-37, pp. 528-537, May 1989.

[7] J.E. Bussoletti, F.T. Johnson, K.W. Sidwell, B.L. Everson, D.P. Young, R.H. Burkart and S.S. Jamant, "EM-TRANAIR: Computer a program for the solution of Maxwell's equations in three dimensions: Volume I, theory manual," Report No. AFWAL-TR-87-3802, prepared by Boeing Military Airplane Co. for the U.S.A.F. Wright Aeronautical Labs, Sept. 1988.

[8] J.D. Collins, J.L. Volakis and J.M. Jin, "A Combined Finite Element-Boundary Integral Formulation for Solution of Two-Dimensional Scattering Problems via CGFFT," IEEE Trans. Antennas Propagat., Nov. 1990.

[9] J.M. Jin and V.V. Liepa, "Application of hybrid finite element method to electromagnetic scattering from coated cylinders," IEEE Trans. Antennas Propagat., Vol. AP-36, pp. 50-54, Jan. 1988.

[10] B.H. McDonald and A. Wexler, "Finite-element solution of unbounded field problems," IEEE Trans. Microwave Theory Tech., Vol. MTT-20, pp. 841-847, Dec. 1972.

[11] K.K. Mei, "Unimoment method of solving antenna and scattering problems," IEEE Trans. Antennas Propagat., Vol. AP-22, pp. 760-766, Nov. 1974.

[12] K.L. Wu, G.Y. Delisle, D.G. Fang and M. Lecours, PIER2: Finite Element and Finite Difference Methods in Electromagnetic Scattering, (Eds. J.A. Kong and M.A. Morgan), Elsevier: New York, Ch. 3, 1990.

[13] J.D. Collins, J.M. Jin and J.L. Volakis, "A combined finite element-boundary element formulation for solution of two-dimensional problems via CGFFT," Electromagnetics, 1990.

[14] J.C. Cavendish, "Automatic triangulation of arbitrary planar domains for the finite element method," Int. J. Numerical Methods Engineering, Vol. 8, pp. 679-696, 1974.

PUBLICATIONS RESULTING FROM THIS RESEARCH

Reports written (to date) related to this Task

- J.D. Collins and J.L. Volakis, "A Combined Finite Element and Boundary Integral Formulation for Solution via CGFFT of 2-Dimensional Scattering Problems." Univ. of Michigan Radiation Lab Technical Report 025921-6-T, August 1989.

- J.M. Jin and J.L. Volakis, "A Finite Element-Boundary Integral Formulation for Scattering by a Cavity-Backed Aperture in a Ground Plane," Univ. of Michigan Radiation Lab Technical Report 025921-10-T, Feb. 1990.

- J.D. Collins and J.L. Volakis, "A Combined Finite Element and Boundary Integral Formulation for Solution via the CGFFT," Univ. of Michigan Radiation Lab Technical Report 025921-11-T, Feb. 1990.

- Changyu Hua, "AUTOMESH-2D User's Manual," University of Michigan Radiation Laboratory Report 025921-15-T, August 1990.

- John Zapp, "User's Manual for Finite Element Mesh Generation Using SDRC IDEAS," University of Michigan Radiation Laboratory Report 025921-16-T.

Papers written (to date) related to this Task

- J.D. Collins, J.L. Volakis and J.M. Jin, "A Combined Finite Element and Boundary Integral Formulation for Solution via CGFFT of 2-Dimensional Scattering Problems," *IEEE Trans. Antennas Propagat.*, Oct. 1990.

- J.M. Jin and J.L. Volakis, "A New Technique for Characterizing Diffraction by an Inhomogeneously Filled Slot of Arbitrary Cross Section in a Thick Conducting Ground Plane," *IEE Electronics Letters*, Vol. 25, No. 17, pp. 1121-1123, 17th August 1989.

- J.M. Jin and J.L. Volakis, "TE Scattering by an Inhomogeneously Filled Aperture in a Thick Conducting Plane," *IEEE Trans. Antennas Propagat.*, 1990.

- J.M. Jin and J.L. Volakis, "TM Scattering by an Inhomogeneously Filled Aperture in a Thick Conducting Plane," *Proc. Inst. Elec. Eng.*, part H, Vol. 137, pp. 153-159, June 1990.

- J.D. Collins, J.M. Jin and J.L. Volakis, "A Combined Finite Element-Boundary Element Formulation for Solution of Two-Dimensional Problems via CGFFT," to appear in *Electromagnetics*.

- J.M. Jin and J.L. Volakis, "Electromagnetic Scattering and Transmission through a Three-Dimensional Slot in a Thick Conducting Plane," submitted to *IEEE Trans. Antennas Propagat.*

- J.M. Jin and J.L. Volakis, "A Finite Element-Boundary Element Method for Scattering by Two and Three Dimensional Structures," submitted to *Proceedings of the IEEE.*

- J.M. Jin and J.L. Volakis, "A Unified Approach to Integral Formulations for Electromagnetic Scattering," submitted to *IEEE Trans. Antennas Propagat.*

Conference Papers/Presentations (to date) related to this Task

- J.D. Collins and J.L. Volakis, "A Combined Finite Element and Boundary Integral Formulation for Solution via CGFFT of 2-Dimensional Scattering Problems," 1989 IEEE AP-S/URSI Symposium, San Jose, CA.

- J.M. Jin and J.L. Volakis, " A FEM/BEM Formulation for a CG-FFT Solution of 2-D Scattering by Grooves and Thick Slots," presented at the 1990 IEEE AP-S/URSI International Symposium, Dallas, TX, URSI Digest p. 260.

- J.M. Jin and J.L. Volakis, "A FEM/BEM Formulation for a CG-FFT Solution of 3-D Scattering by a Cavity-Backed Aperture in a Ground Plane," presented at the 1990 IEEE AP-S/URSI International Symposium, Dallas, TX, AP-S Digest, pp. 1726-1729.

- J.D. Collins and J.L. Volakis, "A Combined Boundary Integral Finite Element Formulation for Solution of Three Dimensional Scattering via Conjugate Gradient Fast Fourier Transform Method," 1990 IEEE AP-S/URSI Symposium, Dallas, TX, URSI Digest p. 263.

- J.M. Jin, J.L. Volakis and J.D. Collins, "A Finite Element Boundary Integral Formulation for Scattering by Two and Three Dimensional Structures," to be presented at the 1990 URSI General Assembly, Session B4, Prague, Chechoslovakia.

- J.M. Jin and J.L. Volakis, "A Finite Element-Boundary Integral Formulation for Scattering by a Three Dimensional Aperture in a Thick Conducting Plane," Submitted to the 4th Biennial IEEE Conference on Electromagnetic Field Computation, Oct. 1990, Toronto.

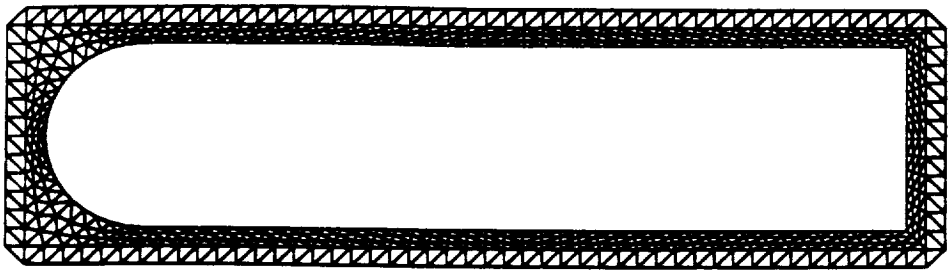

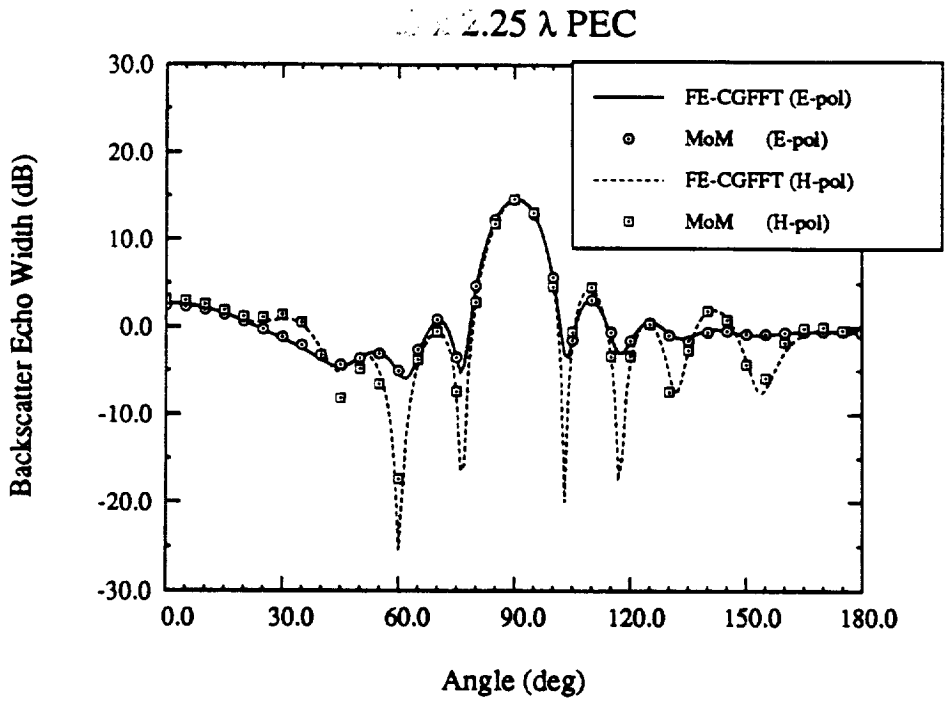

Figure 1: E_z and H_z backscatter echowidth patterns for the illustrated perfectly conducting cylinder.

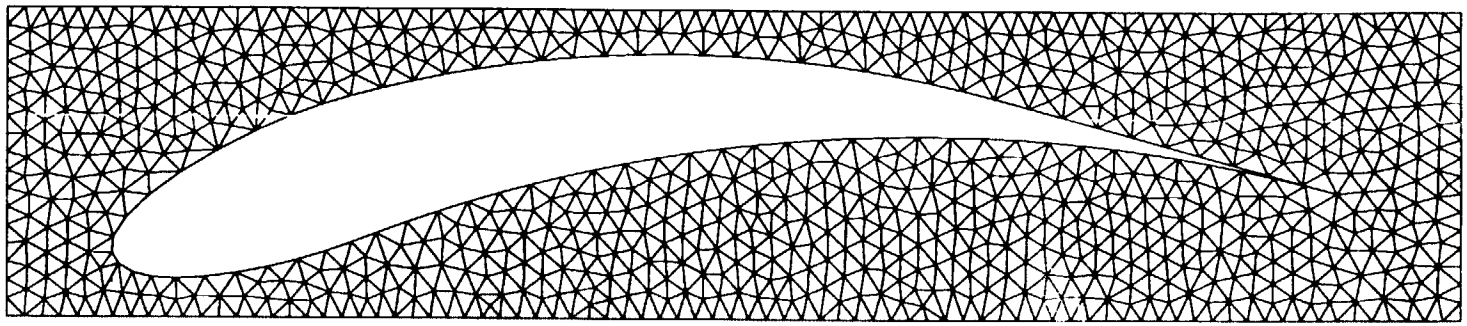

Figure 2(a): Example of a rectangular mesh enclosing a wing cross-section.

COATED OGIVE

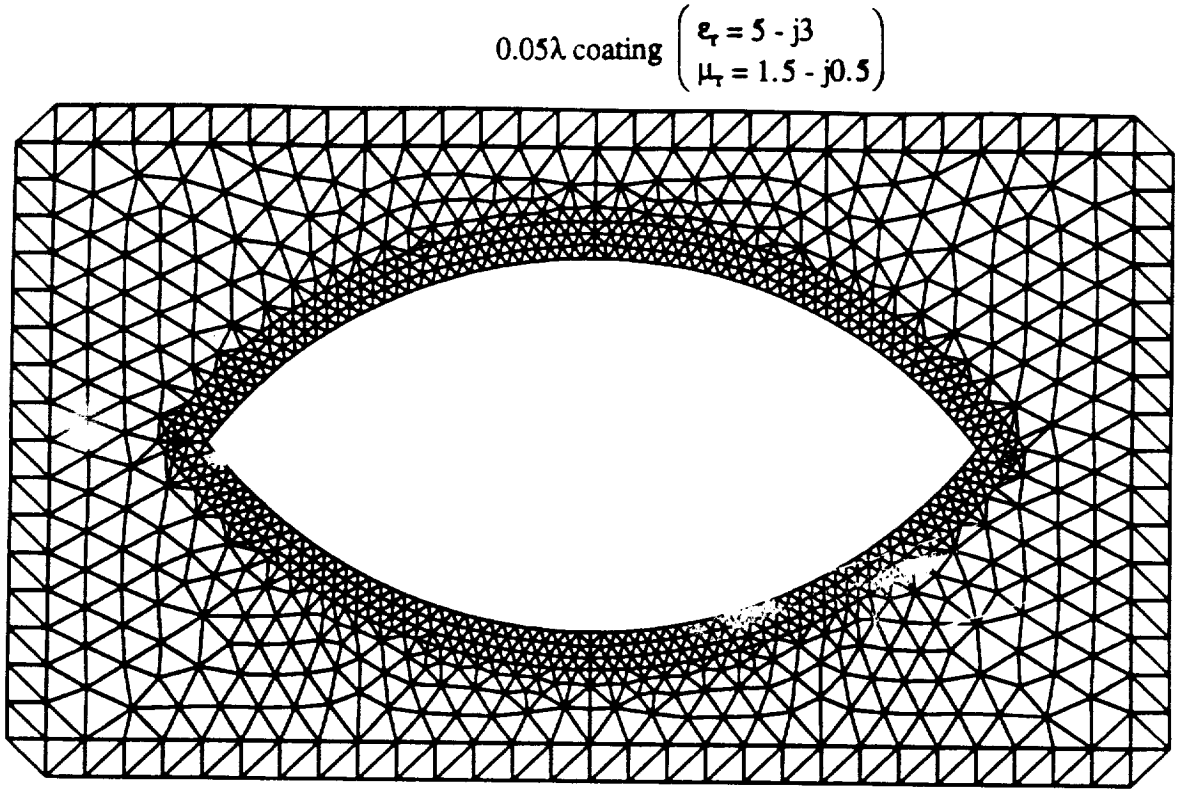

Figure 2(b): Example of a rectangular mesh enclosing a coated ogive.

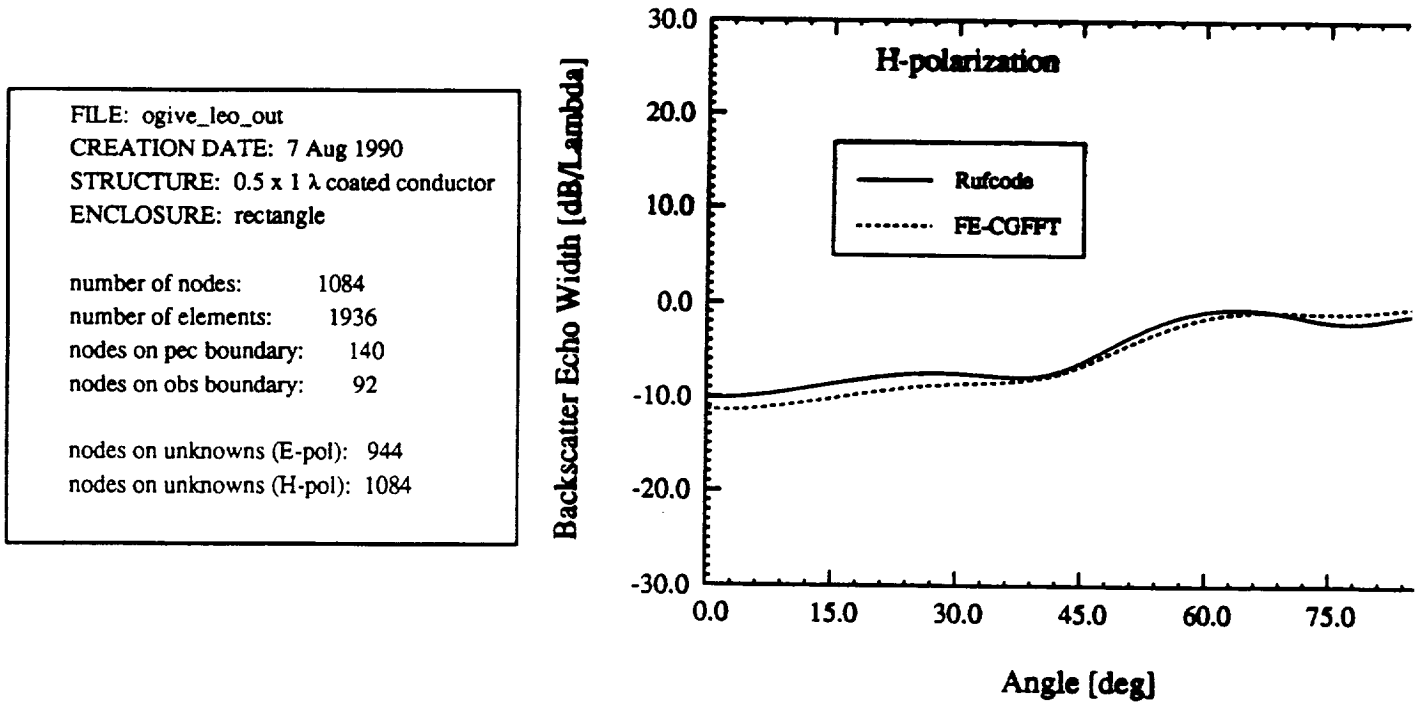

Figure 2(c): H-polarization backscatter pattern for the coated ogive in Fig. 2(b).

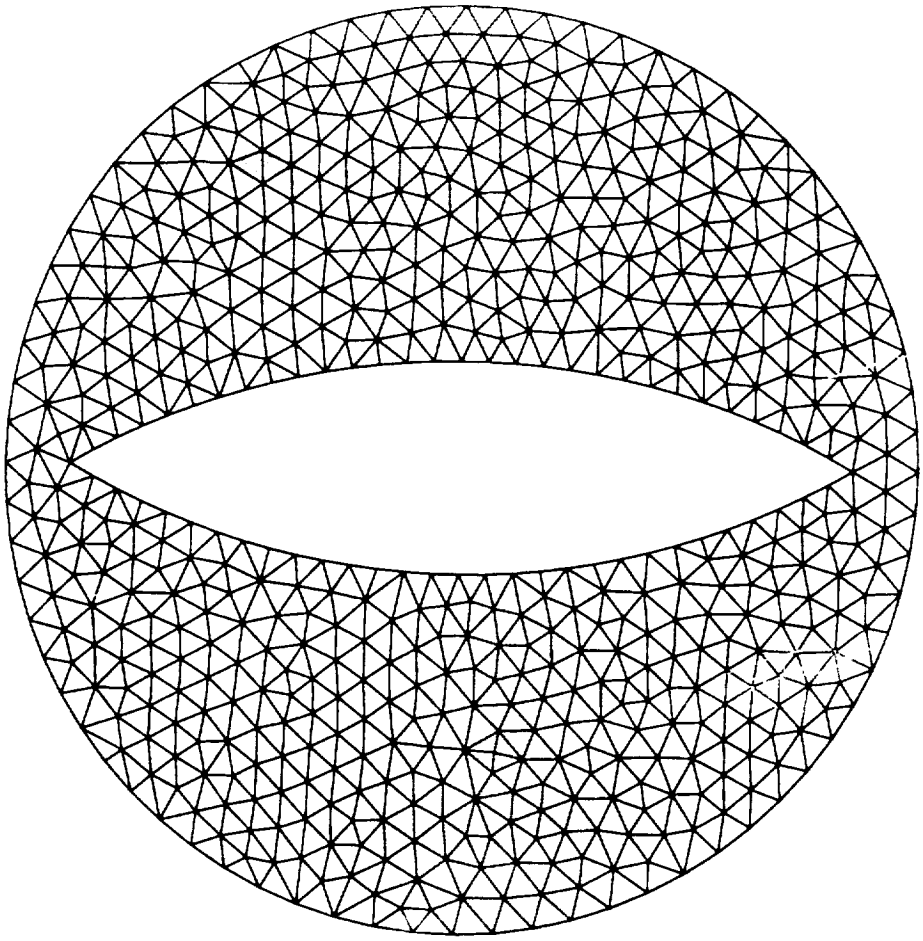

Figure 3: Example of a circular mesh enclosing an ogival cylinder.

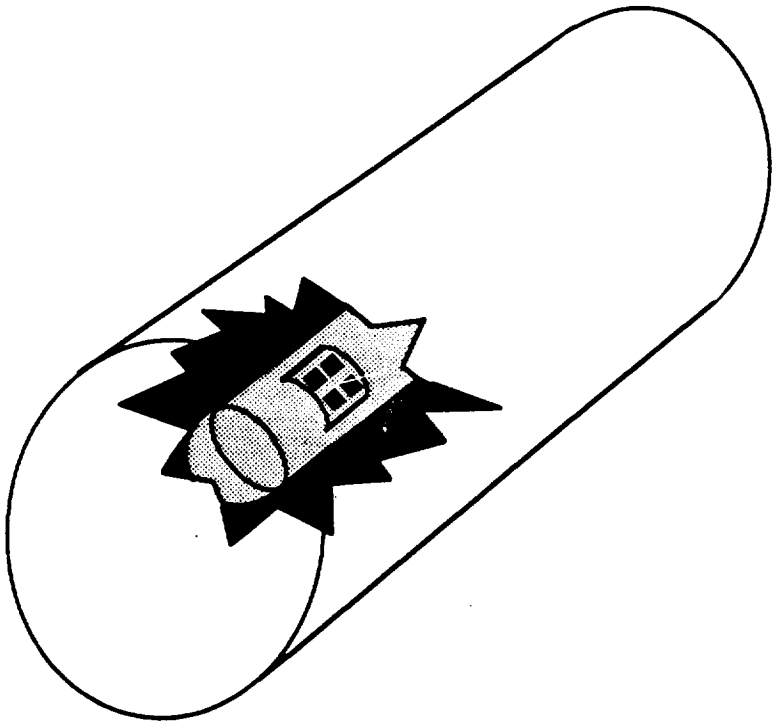

Figure 4: Three-dimensional finite-cylinder enclosure.

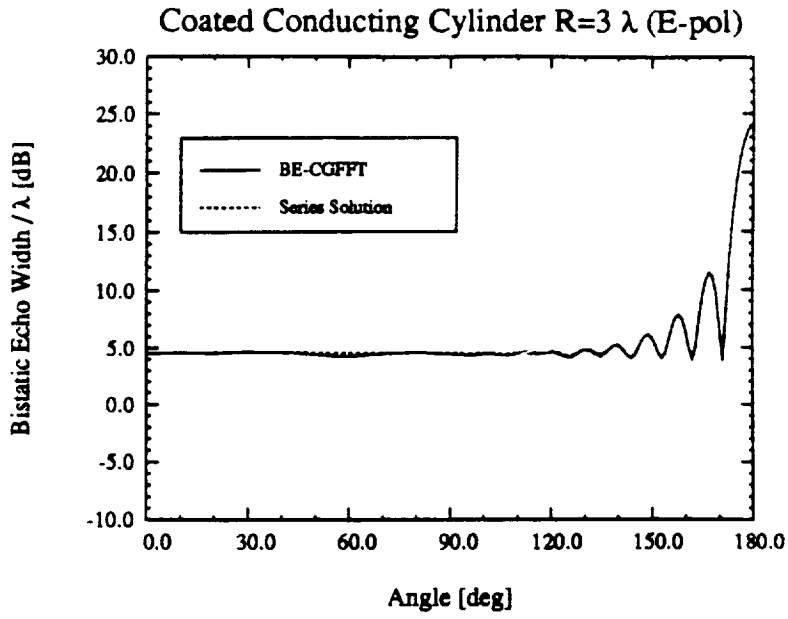

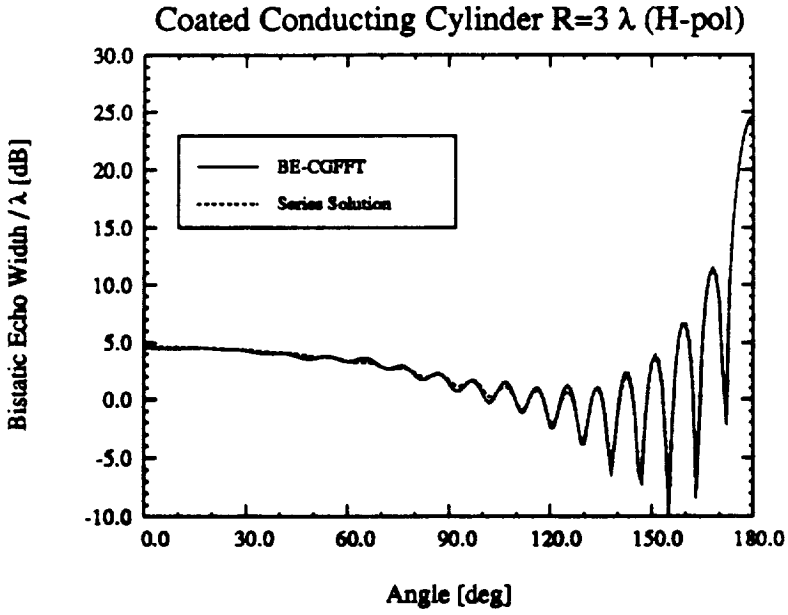

Figure 5: E_z and H_z bistatic echowidth from a coated circular cylinder with a conductor radius of 3λ and coating thickness of 0.05λ with material properites $\varepsilon_r = 5 - j5$, $\mu_r = 1.5 - j0.5$.

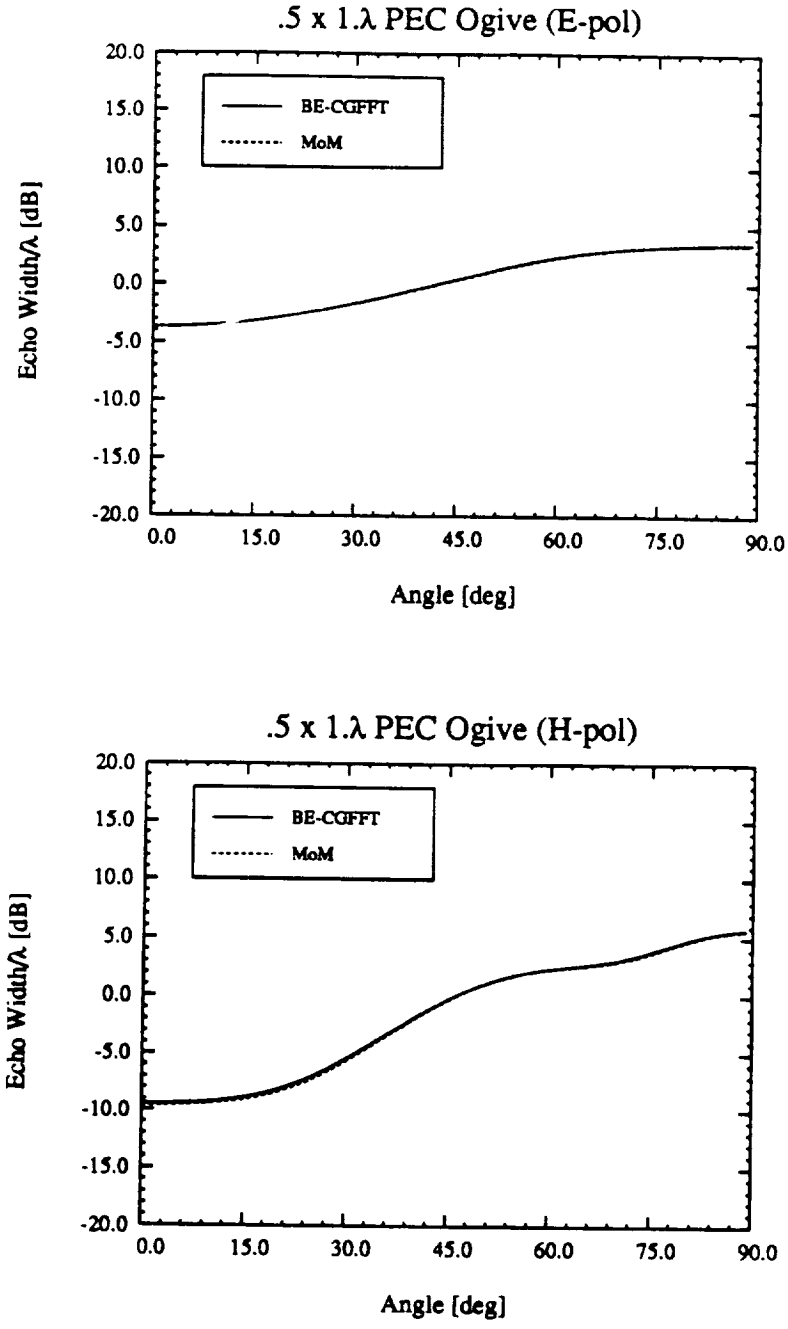

Figure 6: E_z and H_z backscatter echowidth from a $\lambda/2$ x 1λ perfectly conducting ogive.

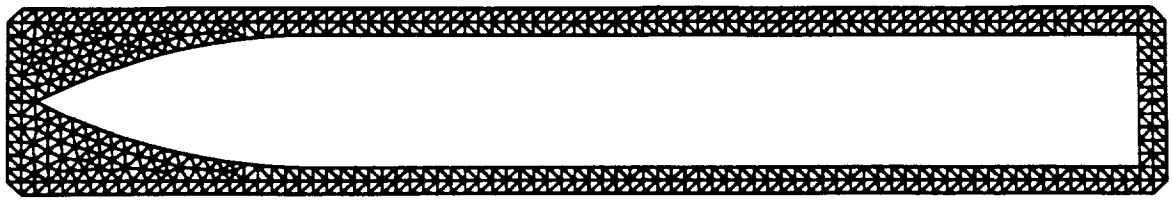

FILE: missile_out
CREATION DATE: 1 Aug 1990
STRUCTURE: missile shape
ENCLOSURE: rectangle

number of nodes: 636
number of elements: 908
nodes on pec boundary: 172
nodes on obs boundary: 192

nodes on unknowns (E-pol): 464
nodes on unknowns (H-pol): 636

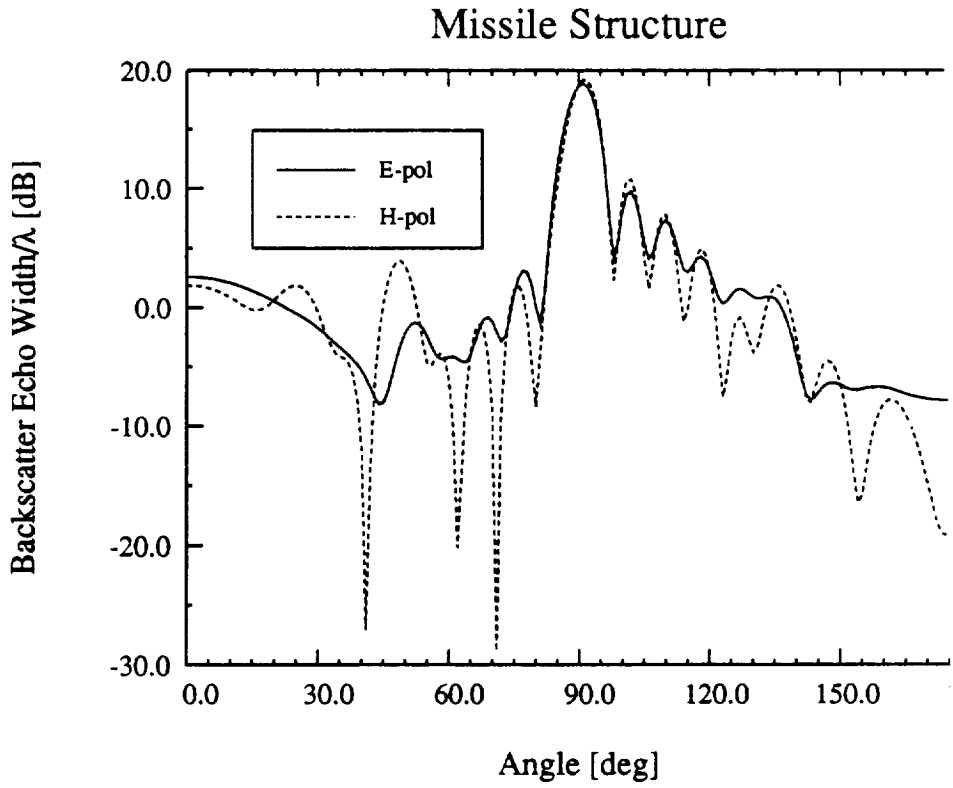

Figure 7: Backscatter patterns for a missile-like perfectly conducting and coated cylinder.

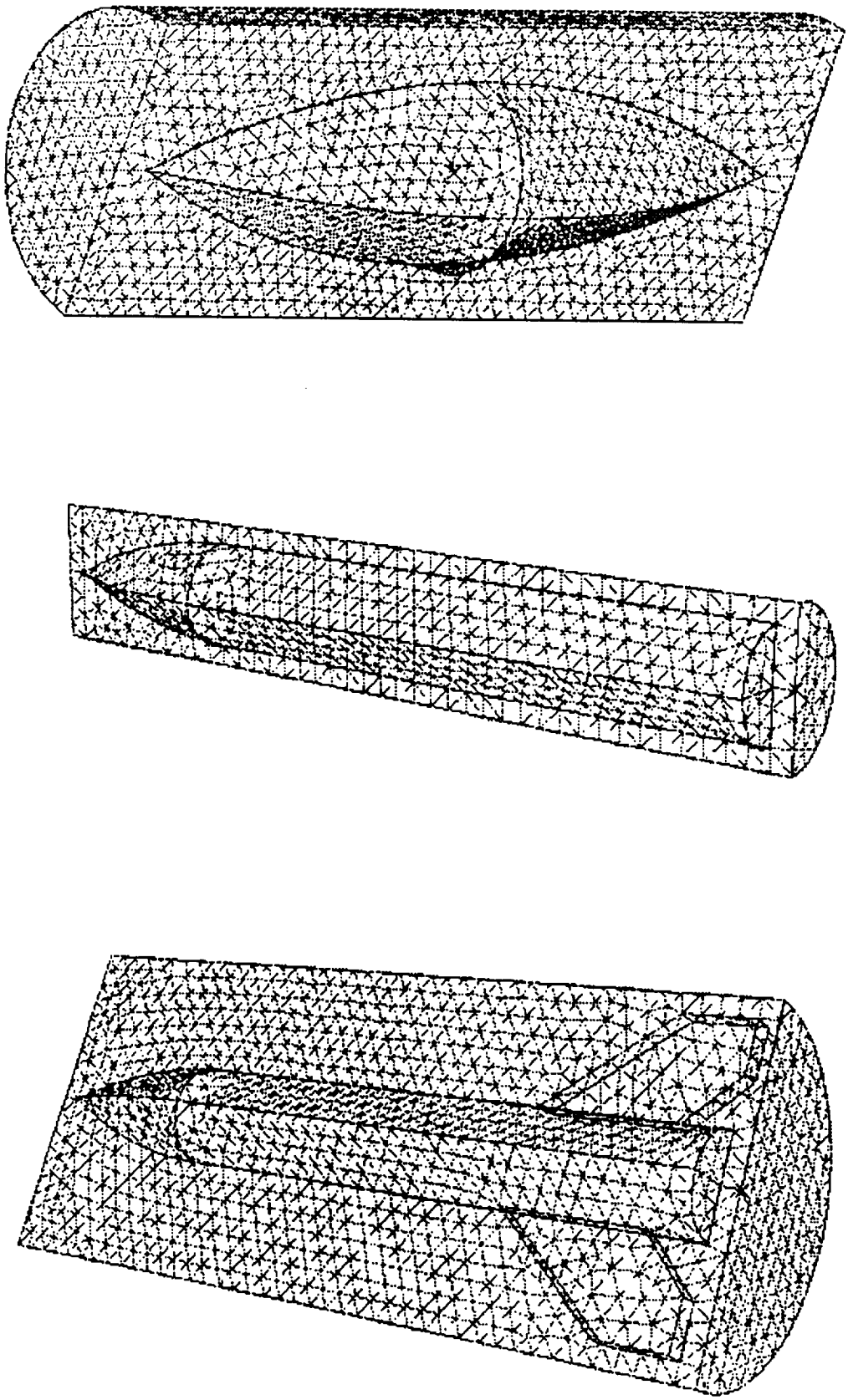

Figure 8: 3D meshes for an ogive and missile-like structures.

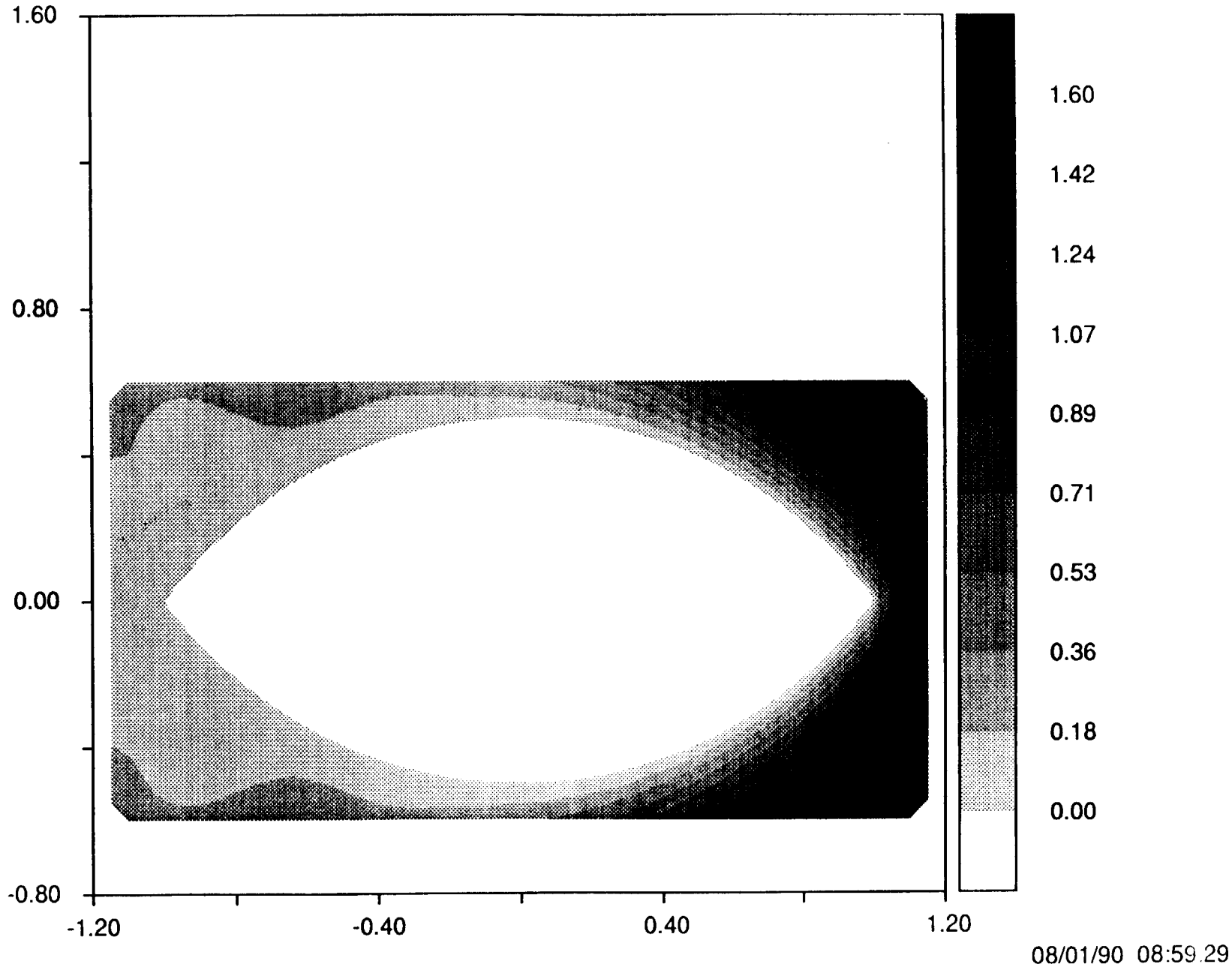

Figure 9: Gray level plot of the field distibution near a PEC ogive with edge-on incidence.

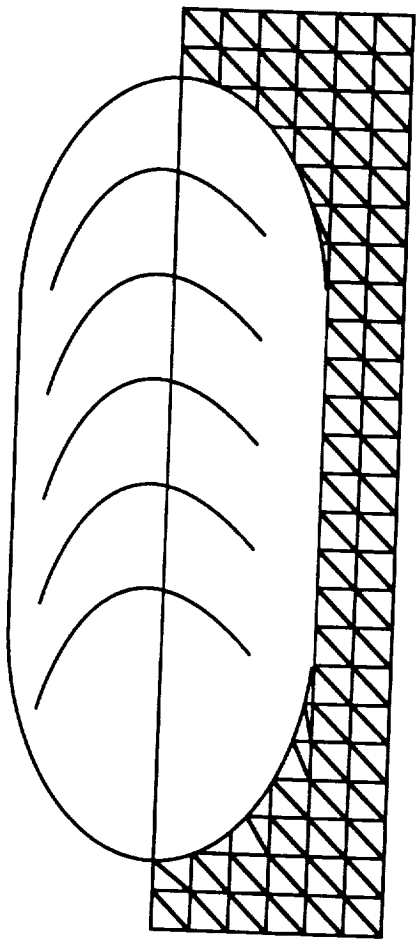

Figure 10: Body of revolution surrounded with a rectangular mesh.

Task Title: Analytical Solutions with Generalized Impedance Boundary Conditions (GIBC)

Investigators: Mark A. Ricoy and John L. Volakis

Period Covered: February 1990 - September 1990

ABSTRACT

The diffraction by a material discontinuity in a thick dielectric/ferrite layer is considered by modelling the layer as a distributed current sheet obeying generalized sheet transition conditions (GSTCs). The sheet currents are then formulated and solved via the standard dual integral equation approach. This yields the diffracted field in terms of unknown constants which underscore the non-uniqueness of the GSTC current sheet representation. The constants are dependent on the geometry and properties of the discontinuity and are determined by enforcing field continuity across the material junction. This requires the field internal to the slab which are determined from the external ones via analytic continuity. Results are given which validate the solution and demonstrate the importance of the constants.

OBJECTIVE

This task involves the use of higher order boundary conditions to generate new solutions in diffraction theory. In particular, diffraction coefficients will be developed for dielectric/magnetic layers and metal-dielectric junctions which are often encountered on airborne vehicles as terminations of coatings and conformal antennas. Solutions for both polarizations will be developed for fairly thick junctions and versatile computer codes will be written and tested. Creeping wave diffraction coefficients will be also developed for multilayered coated cylinders.

PROGRESS

1 Introduction

In scattering, layered materials are often modeled by equivalent sheets satisfying simple boundary/transition conditions. In particular, impenetrable layers are typically replaced by opaque sheets satisfying standard impedance boundary conditions (SIBCs) [1], whereas penetrable layers are

represented by transparent sheets obeying resistive or conductive type transition conditions (STCs) [2]. These simple boundary/transition conditions relate the normal fields to their first normal derivatives through proportionality factors, "impedances" in the SIBC case and "resistivities/conductivities" in the STC case. With this modeling scheme, a discontinuity in layered material is represented by an equivalent sheet discontinuity, whose scattering may be treated via function theoretic techniques such as the Wiener-Hopf method. As is well known, however, these equivalent sheet representations are valid only for very thin or lossy layers and alternative simulations are therefore required to model discontinuities in low loss layers and/or layers of appreciable thickness.

One such approach is to employ generalized impedance boundary conditions (GIBCs) [3] [4] or generalized sheet transition conditions (GSTCs) [5] [6] in place of the usual SIBCs and STCs. The GIBCs and GSTCs are respective generalizations of SIBCs and STCs and permit a more accurate representation of the fields at the surface of the coating or layer. Unlike the SIBCs or STCs, GIBCs and GSTCs include second and possibly higher order derivatives of the field components on the equivalent sheet which are responsible for the higher accuracy of the conditions. The highest derivative kept in the condition defines their order and generally the accuracy of the conditions is analogous to the order. As can be expected, thicker and multilayer coatings require higher order conditions for an accurate simulation and to date a plethora of GIBCs and GSTCs have been derived to model a variety of material coatings and layers [6] [7] [8] [9] [10].

GIBC/GSTC sheets are well suited for characterizing the diffraction by discontinuities in thick coatings or layers. In particular, they can be employed in conjunction with the Wiener-Hopf method or dual integral equation approach without much deviation from the procedure used in connection with the SIBC or STC conditions. However, the resulting solutions obtained in this manner are inherently non-unique [11] [12]. This non-uniqueness cannot be removed with the usual application of the edge condition or the enforcement of reciprocity, which has been used in the past to generate a more physically appealing, if not a unique, solution.

Uniqueness is an obvious requirement of the physical problem and unless resolved it would seriously undermine the usefulness of the conditions. In the case at hand, the non-uniqueness is manifested in the form of unknown

solution constants [12] and this simply points to the fact that additional conditions are required for their specification.

In this paper we demonstrate that the GIBC/GSTC sheet characterization can yield a complete solution when supplemented with certain conditions at the sheet discontinuity which do not require apriori knowledge of the edge fields. As a vehicle in presenting this solution procedure we employ the dual integral equation method to consider the plane wave diffraction by a discontinuous distributed sheet (see Figure 1(b)). This very general model is capable of representing material half-planes, material junctions, and material discontinuities on grounded structures, such as those shown in Figure 2. In addition, a distributed sheet model typically renders the same degree of accuracy as the usual infinitely-thin sheet, but with a lower order condition. It is, therefore, of much practical interest.

In the first part of the paper, the GSTC representation of the distributed sheet discontinuity is used to develop dual integral equations in terms of the unknown spectral functions proportional to the sheet currents. These equations are then solved in the standard manner to yield expressions for the spectral functions in terms of unknown constants, and examples are presented where a proper choice for the constants demonstrates that they recover known solutions. This demonstrates the validity of the presented solution, but in general, the determination of the constants requires the enforcement of additional constraints demanding field continuity across the junction. The development of these conditions and their use in solving for the constants is also presented.

2 Dual Integral Equation Formulation

Consider a distributed sheet of thickness τ illuminated by the plane wave

$$F_{inc} = e^{jk(x\cos\phi_o + y\sin\phi_o)} = \begin{cases} E_{z,inc}, & E_z \text{ polarization}, \\ Z_o H_{z,inc}, & H_z \text{ polarization}, \end{cases} \tag{1}$$

as shown in Figure 1(a). The excitation (1) induces reflected and transmitted fields which are explicitly given by the properties of the distributed sheet. If this sheet models a symmetric slab, then an appropriate GSTC

representation is formally given by [10]

$$\mathcal{U}_{11}^{1}\left(-\frac{\partial x^2}{k^2}\right)\left\{F^{+}-F^{-}\right\}+\frac{j}{k}\mathcal{U}_{12}^{1}\left(-\frac{\partial x^2}{k^2}\right)\left\{\partial y\left[F^{+}+F^{-}\right]\right\}=0,$$

$$-\infty<x<\infty$$

$$\mathcal{U}_{21}^{1}\left(-\frac{\partial x^2}{k^2}\right)\left\{F^{+}+F^{-}\right\}+\frac{j}{k}\mathcal{U}_{22}^{1}\left(-\frac{\partial x^2}{k^2}\right)\left\{\partial y\left[F^{+}-F^{-}\right]\right\}=0,$$

$$-\infty<x<\infty. \qquad (2)$$

in which F is the total field, $F^{\pm}=F(x,y=\pm\tau/2)$, $\partial_x F^{\pm}=\frac{\partial}{\partial x}F(x,y=\pm\tau/2)$, and $\partial y F^{\pm}=\frac{\partial}{\partial y}F(x,y)\,|_{y=\pm\tau/2}$. Also, $\mathcal{U}_{ij}^{1}\left(-\frac{\partial x^2}{k^2}\right)$ are differential operators which operate on the field quantity in the curly brackets, and are finite polynomials in $-\frac{\partial x^2}{k^2}$ whose coefficients depend on the slab modeled by the distributed sheet. To maintain the generality of the solution, the $\mathcal{U}_{ij}^{1}$ operators are left in symbolic form and the reader is referred to [10] for their explicit representation in terms of the material constants and thickness of the layers comprising the modeled slab. In general, the order of $\mathcal{U}_{11}^{1}$ (i.e. the highest derivative present) is usually the same or one more than that of $\mathcal{U}_{12}^{1}$ and similarly the order of $\mathcal{U}_{21}^{1}$ is the same or one more than the order of $\mathcal{U}_{22}^{1}$. Thus, we may define the orders of the GSTCs in (2) to be

$$\begin{aligned} N_1^{odd} &= \text{maximum}\left\{\text{ order of }\mathcal{U}_{11}^{1}\left(\lambda^2\right),1+\text{ order of }\mathcal{U}_{12}^{1}\left(\lambda^2\right)\right\} \\ N_1^{even} &= \text{maximum}\left\{\text{ order of }\mathcal{U}_{21}^{1}\left(\lambda^2\right),1+\text{ order of }\mathcal{U}_{22}^{1}\left(\lambda^2\right)\right\} \end{aligned} \qquad (3)$$

The reflected and transmitted fields may now be easily determined by employing (2) to find

$$F_{refl} = R_1 e^{jk(x\cos\phi_o - y\sin\phi_o)} \qquad (4)$$

$$F_{tran} = T_1 e^{jk(x\cos\phi_o + y\sin\phi_o)} \qquad (5)$$

in which R_1 and T_1 are the reflection and transmission coefficients, respectively, and are given as

$$R_1 = \frac{e^{jk\tau\sin\phi_o}}{2}\left[R_1^{even}+R_1^{odd}\right] \qquad (6)$$

$$T_1 = \frac{e^{jk\tau\sin\phi_o}}{2}\left[R_1^{even}-R_1^{odd}\right]. \qquad (7)$$

with

$$R_1^{even} = \frac{\sin\phi_o \mathcal{U}_{22}^1(\cos^2\phi_o) - \mathcal{U}_{21}^1(\cos^2\phi_o)}{\sin\phi_o \mathcal{U}_{22}^1(\cos^2\phi_o) + \mathcal{U}_{21}^1(\cos^2\phi_o)} \tag{8}$$

$$R_1^{odd} = \frac{\sin\phi_o \mathcal{U}_{12}^1(\cos^2\phi_o) - \mathcal{U}_{11}^1(\cos^2\phi_o)}{\sin\phi_o \mathcal{U}_{12}^1(\cos^2\phi_o) + \mathcal{U}_{11}^1(\cos^2\phi_o)}. \tag{9}$$

We remark that in (8) and (9), $\mathcal{U}_{ij}^1(\cos^2\phi_o)$ now represent simple polynomial functions in $\cos^2\phi_o$, since $-\partial x^2/k^2 = \cos^2\phi_o$ in view of the field expressions (4) and (5).

Consider now the case where the right half of the distributed sheet in Figure 1(a) is replaced by another sheet of the same thickness, but of different properties, as illustrated in Figure 1(b). The GSTC representation of this modified sheet is

$$\begin{aligned}
\mathcal{U}_{11}^1\left(-\frac{\partial x^2}{k^2}\right)\left\{F^+ - F^-\right\} + \frac{j}{k}\mathcal{U}_{12}^1\left(-\frac{\partial x^2}{k^2}\right)\left\{\partial y\left[F^+ + F^-\right]\right\} &= 0 \\
\mathcal{U}_{21}^1\left(-\frac{\partial x^2}{k^2}\right)\left\{F^+ + F^-\right\} + \frac{j}{k}\mathcal{U}_{22}^1\left(-\frac{\partial x^2}{k^2}\right)\left\{\partial y\left[F^+ - F^-\right]\right\} &= 0,
\end{aligned} \tag{10}$$

for $-\infty < x < 0$ and

$$\begin{aligned}
\mathcal{U}_{11}^2\left(-\frac{\partial x^2}{k^2}\right)\left\{F^+ - F^-\right\} + \frac{j}{k}\mathcal{U}_{12}^2\left(-\frac{\partial x^2}{k^2}\right)\left\{\partial y\left[F^+ + F^-\right]\right\} &= 0 \\
\mathcal{U}_{21}^2\left(-\frac{\partial x^2}{k^2}\right)\left\{F^+ + F^-\right\} + \frac{j}{k}\mathcal{U}_{22}^2\left(-\frac{\partial x^2}{k^2}\right)\left\{\partial y\left[F^+ - F^-\right]\right\} &= 0,
\end{aligned} \tag{11}$$

for $0 < x < \infty$, where the superscripts 1 and 2 distinguish the left- and right-hand sheets, respectively. Referring to our previous discussion, the orders of the right hand side GSTCs are given as

$$\begin{aligned}
N_2^{odd} &= \max\left\{\text{order of } \mathcal{U}_{11}^2\left(\lambda^2\right) \text{ in } \lambda, 1 + \text{order of } \mathcal{U}_{12}^2\left(\lambda^2\right) \text{ in } \lambda\right\} \\
N_2^{even} &= \max\left\{\text{order of } \mathcal{U}_{21}^2\left(\lambda^2\right) \text{ in } \lambda, 1 + \text{order of } \mathcal{U}_{22}^2\left(\lambda^2\right) \text{ in } \lambda\right\}.
\end{aligned} \tag{12}$$

The modified right hand side sheet induces a scattered field F_s in the presence of the excitation (1), and the total field can be represented as

$$F = \begin{cases} F_{inc} + F_{refl} + F_s & y > \tau/2 \\ F_{tran} + F_s & y < \tau/2 \end{cases} \tag{13}$$

where F_s is the unknown scattered field in the region $|y| > \tau/2$ and can be expressed as [13] [14]

$$\begin{aligned} F^s(x,y) &= \int_C \left[\frac{|y|}{y} P_{odd}(\cos\alpha) + P_{even}(\cos\alpha) \right] \\ &\cdot \; e^{-jk\sin\alpha(|y|-\tau/2)} e^{-jkx\cos\alpha} d\alpha. \end{aligned} \tag{14}$$

where C is a contour in the complex α plane, such that $\lambda = \cos\alpha$ runs from $-\infty$ to ∞ as shown in Figure 3. In this, the spectral functions $P_{odd}(\cos\alpha)$ and $P_{even}(\cos\alpha)$ are directly related to the Fourier transforms of the unknown equivalent currents

$$J_{odd} = F_s^+ - F_s^- \tag{15}$$

$$J_{even} = F_s^+ + F_s^-, \tag{16}$$

via the relations

$$J_{odd}(x) = 2\int_{-\infty}^{\infty} P_{odd}(\lambda)\, e^{-jkx\lambda} \frac{d\lambda}{\sqrt{1-\lambda^2}} \tag{17}$$

$$J_{even}(x) = 2\int_{-\infty}^{\infty} P_{even}(\lambda)\, e^{-jkx\lambda} \frac{d\lambda}{\sqrt{1-\lambda^2}}. \tag{18}$$

Substituting (1), (4), (5), (13) and (14) into the transition conditions (11) and (12), and introducing the transformation $\lambda = \cos\alpha$ (see Figure 3) yields

$$\int_{-\infty}^{\infty} \mathcal{G}_1^{odd}\left(\lambda^2\right) P_{odd}(\lambda)\, e^{-jkx\lambda} \frac{d\lambda}{\sqrt{1-\lambda^2}} = 0 \tag{19}$$

$$\int_{-\infty}^{\infty} \mathcal{G}_1^{even}\left(\lambda^2\right) P_{even}(\lambda)\, e^{-jkx\lambda} \frac{d\lambda}{\sqrt{1-\lambda^2}} = 0, \tag{20}$$

for $x < 0$ and

$$\int_{-\infty}^{\infty} 2\mathcal{G}_2^{odd}\left(\lambda^2\right) P_{odd}\left(\lambda\right) e^{-jkx\lambda} \frac{d\lambda}{\sqrt{1-\lambda^2}}$$

$$= \frac{2\sin\phi_o e^{jkx\lambda_o} e^{jk\tau/2\sin\phi_o} Z_{odd}\left(\lambda_o^2\right)}{\mathcal{G}_1^{odd}\left(\lambda_o^2\right)} \tag{21}$$

$$\int_{-\infty}^{\infty} 2\mathcal{G}_2^{even}\left(\lambda^2\right) P_{even}\left(\lambda\right) e^{-jkx\lambda} \frac{d\lambda}{\sqrt{1-\lambda^2}}$$

$$= \frac{2\sin\phi_o e^{jkx\lambda_o} e^{jk\tau/2\sin\phi_o} Z_{even}\left(\lambda_o^2\right)}{\mathcal{G}_1^{even}\left(\lambda_o^2\right)} \tag{22}$$

for $x > 0$, where $\lambda_o = \cos\phi_o$ and

$$\mathcal{G}_1^{odd}\left(\lambda^2\right) = \mathcal{U}_{11}^1\left(\lambda^2\right) + \sqrt{1-\lambda^2}\mathcal{U}_{12}^1\left(\lambda^2\right) \tag{23}$$

$$\mathcal{G}_1^{even}\left(\lambda^2\right) = \mathcal{U}_{21}^1\left(\lambda^2\right) + \sqrt{1-\lambda^2}\mathcal{U}_{22}^1\left(\lambda^2\right) \tag{24}$$

$$\mathcal{G}_2^{odd}\left(\lambda^2\right) = \mathcal{U}_{11}^2\left(\lambda^2\right) + \sqrt{1-\lambda^2}\mathcal{U}_{12}^2\left(\lambda^2\right) \tag{25}$$

$$\mathcal{G}_2^{even}\left(\lambda^2\right) = \mathcal{U}_{21}^2\left(\lambda^2\right) + \sqrt{1-\lambda^2}\mathcal{U}_{22}^2\left(\lambda^2\right) \tag{26}$$

$$Z_{odd}\left(\lambda_o^2\right) = \left[\mathcal{U}_{11}^1\left(\lambda_o^2\right)\mathcal{U}_{12}^2\left(\lambda_o^2\right) - \mathcal{U}_{12}^1\left(\lambda_o^2\right)\mathcal{U}_{11}^2\left(\lambda_o^2\right)\right] \tag{27}$$

$$Z_{even}\left(\lambda_o^2\right) = \left[\mathcal{U}_{21}^1\left(\lambda_o^2\right)\mathcal{U}_{22}^2\left(\lambda_o^2\right) - \mathcal{U}_{22}^1\left(\lambda_o^2\right)\mathcal{U}_{21}^2\left(\lambda_o^2\right)\right]. \tag{28}$$

Equations (19) with (21) and (20) with (22) form two uncoupled sets of integral equations, sufficient to yield a solution for the unknown spectra $P_{odd}\left(\lambda\right)$ and $P_{even}\left(\lambda\right)$. Clearly, because of the similarity between the two sets of equations, once a solution for $P_{odd}\left(\lambda\right)$ is found, the corresponding one for $P_{even}\left(\lambda\right)$ follows by inspection.

3 Solution of the Diffracted Field

Upon a solution of the dual integral equations (19) and (21) we obtain

$$P_{odd}(\lambda) = \frac{j}{2\pi}\frac{\sin\phi}{\lambda+\lambda_o}\frac{\sqrt{1-\lambda^2}}{\mathcal{G}_{1-}^{odd}(\lambda)\mathcal{G}_{1-}^{odd}(\lambda_o)\mathcal{G}_{2+}^{odd}(\lambda)\mathcal{G}_{2+}^{odd}(\lambda_o)}\frac{e^{jk\tau/2\sin\phi_o}}{}$$
$$\cdot\left[Z_{odd}\left(\lambda_o^2\right)\frac{E_{odd}(\lambda)}{E_{odd}(-\lambda_o)}+\sum_{m=1}^{\widetilde{N}_{odd}-1}\sum_{n=0}^{\widetilde{N}_{odd}-1-m}a_{mn}(\lambda+\lambda_o)^m(\lambda\lambda_o)^n\right] \quad (29)$$

where we have assumed that $J_{odd}(x)\sim x^{S_{odd}}$ as $x\to 0$ with $0<S_{odd}<1$. In this, $\widetilde{N}_{odd}=int\{1/2(N_{odd}^1+N_{odd}^2+1)\}$, and a_{mn} are arbitrary constants as yet undetermined, and correspond to the coefficients of the polynomial resulting from the application of Liouville's theorem. The chosen symmetric form of this polynomial is not unique but will be found most useful later in constructing a reciprocal form for $P_{odd}(\lambda)$. Also, $G_{1+}(\lambda)$ are Wiener-Hopf split function regular in the upper (+) or lower (-) half of the λ-plane and satisfy the relation

$$G_1(\lambda^2)=G_{1+}(\lambda)G_{1-}(\lambda) \quad (30)$$

(see Appendix). Similarly, $G_{2\pm}(\lambda)$ are the corresponding split functions associated with $G_2(\lambda^2)$. Finally, $E_{odd}(\lambda)$ is some entire function behaving no worse than $|\lambda|^{(N_{odd}^1+N_{odd}^2)/2-S_{odd}}$ and can take any of the forms

$$E_{odd}(\lambda) = \begin{cases} Z_{odd}(-\lambda\lambda_o) & \text{or} \\ Z_{odd}^-(\lambda) & \text{or} \\ Z_{odd}^+(\lambda) & \end{cases} \quad (31)$$

where $Z^{\pm}(\lambda)$ are again upper and lower functions satisfying the relation

$$Z(\lambda^2)=Z^+(\lambda)Z^-(\lambda) \quad (32)$$

Following a similar procedure we obtain $P_{even}(\lambda)$ as

$$P_{even}(\lambda) = \frac{j}{2\pi}\frac{\sin\phi_o\sqrt{1-\lambda^2}}{\lambda+\lambda_o}\frac{e^{jk\tau/2\sin\phi_o}}{\mathcal{G}_{1-}^{even}(\lambda)\mathcal{G}_{1-}^{even}(\lambda_o)\mathcal{G}_{2+}^{even}(\lambda)\mathcal{G}_{2+}^{even}(\lambda_o)}$$
$$\cdot\left[Z_{even}\left(\lambda_o^2\right)\frac{E_{even}(\lambda)}{E_{even}(-\lambda_o)}+\sum_{m=1}^{\widetilde{N}_{even}-1}\sum_{n=0}^{\widetilde{N}_{even}-1-m}b_{mn}(\lambda+\lambda_o)^m(\lambda\lambda_o)^n\right] \quad (33)$$

with $E_{even}(\lambda)$, $\widetilde{N}_{even}$ and b_{mn} being the counterparts of $E_{odd}(\lambda)$, $\widetilde{N}_{odd}$ and a_{mn}, respectively. Taking into account the choices (31), we may substitute (29) and (33) into (14) and subsequently perform a steepest descent path evaluation to obtain for $\rho \to \infty$ (all surface wave contributions are neglected in this evaluation)

$$F(\rho,\phi) \sim [D_{odd}(\phi,\phi_o) + D_{even}(\phi,\phi_o)] \frac{e^{-jk\rho}}{\sqrt{k\rho/2\pi}} \tag{34}$$

where (ρ,ϕ) are the usual cylindrical coordinates and $D_{odd}(\phi,\phi_o)+D_{even}(\phi,\phi_o)$ is the far zone diffraction coefficient symmetric with respect to ϕ and ϕ_o. We have

$$\begin{aligned} D_{odd}(\phi,\phi_o) &= -\frac{e^{-j\pi/4}}{2\pi}\frac{\sin\phi_o \sin\phi}{\cos\phi+\cos\phi_o} \\ &\cdot \frac{e^{jk\tau/2(\sin\phi_o+|\sin\phi|)}}{\mathcal{G}_{1-}^{odd}(\cos\phi)\,\mathcal{G}_{1-}^{odd}(\cos\phi_o)\,\mathcal{G}_{2+}^{odd}(\cos\phi)\,\mathcal{G}_{2+}^{odd}(\cos\phi_o)} \\ &\cdot \left[\widetilde{Z}_{odd}(\cos\phi,\cos\phi_o) + \sum_{m=1}^{\widetilde{N}_{odd}-1}\sum_{n=0}^{\widetilde{N}_{odd}-1-m} a_{mn} \right. \\ &\left. \cdot (\cos\phi+\cos\phi_o)^m (\cos\phi\cos\phi_o)^n \right] \end{aligned} \tag{35}$$

$$\begin{aligned} D_{even}(\phi,\phi_o) &= -\frac{e^{-j\pi/4}}{2\pi}\frac{\sin\phi_o|\sin\phi|}{\cos\phi+\cos\phi_o} \\ &\cdot \frac{e^{jk\tau/2(\sin\phi_o+|\sin\phi|)}}{\mathcal{G}_{1-}^{even}(\cos\phi)\,\mathcal{G}_{1-}^{even}(\cos\phi_o)\,\mathcal{G}_{2+}^{even}(\cos\phi)\,\mathcal{G}_{2+}^{even}(\cos\phi_o)} \\ &\cdot \left[\widetilde{Z}_{even}(\cos\phi,\cos\phi_o) + \sum_{m=1}^{\widetilde{N}_{even}-1}\sum_{n=0}^{\widetilde{N}_{even}-1-m} b_{mn} \right. \\ &\left. \cdot (\cos\phi+\cos\phi_o)^m (\cos\phi\cos\phi_o)^n \right] \end{aligned} \tag{36}$$

in which the functions $\tilde{Z}_{odd,even}(\cos\phi, \cos\phi_o)$ are given by (see (31))

$$\tilde{Z}_{odd}(\cos\phi, \cos\phi_o) = \begin{cases} Z_{odd}(-\cos\phi\cos\phi_o) & \text{or} \\ Z^{-}_{odd}(\cos\phi)\, Z^{-}_{odd}(\cos\phi_o) & \text{or} \\ Z^{+}_{odd}(\cos\phi)\, Z^{+}_{odd}(\cos\phi_o) & \end{cases} \tag{37}$$

$$\tilde{Z}_{even}(\cos\phi, \cos\phi_o) = \begin{cases} Z_{even}(-\cos\phi\cos\phi_o) & \text{or} \\ Z^{-}_{even}(\cos\phi)\, Z^{-}_{even}(\cos\phi_o) & \text{or} \\ Z^{+}_{even}(\cos\phi)\, Z^{+}_{even}(\cos\phi_o) & \end{cases} \tag{38}$$

Because the above three choices for $\tilde{Z}_{odd}$ and $\tilde{Z}_{even}$ differ only by terms of the form $(\cos\phi + \cos\phi_o)^m (\cos\phi\cos\phi_o)^n$, it is immaterial which of them we choose, although one of the choices may likely lead to a more compact representation. Nevertheless, regardless of the choice of $\tilde{Z}_{odd}$ and $\tilde{Z}_{even}$, one is still faced with the determination of the unknown constants a_{mn} and b_{mn} in (35) and (36), repectively. These are a manifestation of the non-uniqueness of the finite-order GSTC sheet model employed herein, and their explicit determination requires the introduction of additional constraints pertaining to the physics of the problem. Before we consider their determination for the general case, we first look at a specific example, that of diffraction by a thin single layer junction.

4 Diffraction by Thin Single Layer Discontinuous Slabs

The diffraction coefficient given by (35) and (36) is very general and can model a wide variety of geometries. To check its validity, display its versatility, and assess the relative importance of the unknown constants, we consider the thin material-to-material junction of thickness $2w$ as shown in Figure 4. The slab will be modelled by a sheet of thickness $2(w - w_s)$ and with a proper choice of the material parameters this geometry can reduce to junctions whose diffracted field is available, thus, permitting some validation of our solution.

If the left hand side of the slab, in addition to being thin, is also associated with low index of refraction, it may be modeled by a low contrast GSTC sheet. Thus, an $O(w^1, w_s^1)$ approximation with terms of $O(w_s w)$ neglected is sufficient for the representation of the operators or polynomials

$\mathcal{U}^1_{ij}$. In particular, we have

$$\begin{aligned}
\mathcal{U}^1_{11}\left(-\partial x^2/k^2\right) &= 1 \\
\mathcal{U}^1_{12}\left(-\partial x^2/k^2\right) &= jk\left(u_1 w - w_s\right) \\
\mathcal{U}^1_{21}\left(-\partial x^2/k^2\right) &= jk\left(\frac{w\epsilon_1\mu_1}{u_1} - w_s\right) + \frac{j}{k}\left(\frac{w}{u_1} - w_s\right)\partial x^2 \\
\mathcal{U}^1_{22}\left(-\partial x^2/k^2\right) &= 1
\end{aligned} \tag{39}$$

where ϵ_1 and μ_1 are the relative permittivity and permeability of the left hand slab, respectively, and

$$u_1 = \begin{cases} \mu_1, & E_z \text{ polarization} \\ \epsilon_1 & H_z \text{ polarization} \end{cases} . \tag{40}$$

Also, when $w_s = w$, these are simply the transition conditions derived first by Weinstein [5] and later by Senior and Volakis [6]. The corresponding polynomials to be employed in (23) - (28) are given by

$$\begin{aligned}
\mathcal{U}^1_{11}\left(-\cos\phi\cos\phi_o\right) &= 1 \\
\mathcal{U}^1_{12}\left(-\cos\phi\cos\phi_o\right) &= jk\left(u_1 w - w_s\right) \\
\mathcal{U}^1_{21}\left(-\cos\phi\cos\phi_o\right) &= jk\left(\frac{w\epsilon_1\mu_1}{u_1} - w_s\right) + jk\left(\frac{w}{u_1} - w_s\right)\cos\phi\cos\phi_o \\
\mathcal{U}^1_{22}\left(-\cos\phi\cos\phi_o\right) &= 1
\end{aligned} \tag{41}$$

Incorporating these into (35) and (36) and setting

$$\tilde{Z}_{odd}\left(\cos\phi, \cos\phi_o\right) = Z_{odd}\left(-\cos\phi\cos\phi_o\right) \tag{42}$$

$$\tilde{Z}_{even}\left(\cos\phi, \cos\phi_o\right) = Z_{even}\left(-\cos\phi\cos\phi_o\right) \tag{43}$$

yields

$$\begin{aligned}
D_{odd}\left(\phi, \phi_o\right) &= -\frac{e^{-j\pi/4}}{2\pi}\frac{\sin\phi_o\sin\phi}{\cos\phi + \cos\phi_o}e^{jk\tau/2(\sin\phi_o + |\sin\phi|)} \\
&\cdot \frac{\mathcal{U}^2_{12}\left(-\cos\phi\cos\phi_o\right) - jk\left(u_1 w - w_s\right)\mathcal{U}^2_{11}\left(-\cos\phi\cos\phi_o\right)}{M_-\left(\cos\phi; \gamma^{odd,1}\right) M_-\left(\cos\phi_o; \gamma^{odd,1}\right) \mathcal{G}^{odd}_{2+}\left(\cos\phi\right) \mathcal{G}^{odd}_{2+}\left(\cos\phi_o\right)}
\end{aligned} \tag{44}$$

$$D_{even}(\phi,\phi_o) = -\frac{e^{-j\pi/4}}{2\pi}\frac{\sin\phi_o|\sin\phi|}{\cos\phi+\cos\phi_o}e^{jk\tau/2(\sin\phi_o+|\sin\phi|)}$$

$$\cdot\left\{\frac{[\alpha_1+\alpha_2\cos\phi\cos\phi_o]\mathcal{U}_{22}^2(-\cos\phi\cos\phi_o)-\mathcal{U}_{21}^2(-\cos\phi\cos\phi_o)}{\alpha_3\left[\prod_{m=1}^{2}M_-\left(\cos\phi;\gamma_m^{even,1}\right)M_-\left(\cos\phi_o;\gamma_m^{even,1}\right)\right]\mathcal{G}_{2+}^{even}(\cos\phi)\mathcal{G}_{2+}^{even}(\cos\phi_o)}\right.$$

$$\left.+\frac{b_{10}(\cos\phi+\cos\phi_o)}{\alpha_3\left[\prod_{m=1}^{2}M_-\left(\cos\phi;\gamma_m^{even,1}\right)M_-\left(\cos\varphi_o;\gamma_m^{even,1}\right)\right]\mathcal{G}_{2+}^{even}(\cos\phi)\mathcal{G}_{2+}^{even}(\cos\phi_o)}\right\} \tag{45}$$

where the split function $M_-(\cos\phi;\gamma)$ is given in the Appendix,

$$\begin{aligned}\alpha_1 &= jk\left(\frac{w\epsilon_1\mu_1}{u_1}-w_s\right)\\ \alpha_2 &= jk\left(\frac{w}{u_1}-w_s\right)\\ \alpha_3 &= \frac{jkw}{u_1}(\epsilon_1\mu_1-1)\end{aligned} \tag{46}$$

and

$$\begin{aligned}\gamma^{odd,1} &= \frac{-j}{k(u_1w-w_s)}\\ \gamma_{1,2}^{even,1} &= \frac{u_1\pm\sqrt{u_1^2+4k^2w(\epsilon_1\mu_1-1)(w-u_1w_s)}}{2jk(w-w_su_1)}\end{aligned} \tag{47}$$

with $\gamma^{odd\ or\ even}$ are associated with possible surface wave poles. To complete the definition of (44) and (45), the functions associated with the right hand side properties of the slab (i.e. those functions with the superscript 2) must be specified and Tables 1 and 2 provide explicit expressions for the functions $\mathcal{U}_{ij}^2(-\cos\phi\cos\phi_o)$, $\mathcal{G}_{2+}^{odd}(\cos\phi)\,\mathcal{G}_{2+}^{odd}(\cos\phi_o)$ and $\mathcal{G}_{2+}^{even}(\cos\phi)\;\mathcal{G}_{2+}^{even}(\cos\phi_o)$ terms. By edge condition considerations, all of the constants a_{mn} and b_{mn} have been set to zero except b_{10} appearing in the definition of D_{even}, which is non-zero unless the right hand side slab is a PEC/PMC under an E_z/H_z excitation (see Table 2).

By invoking image theory the diffraction coefficient for the grounded metal- dielectric join, shown in Figure 5 is given by

$$D_{rs}(\cos\phi,\cos\phi_o) = 2D_{even}(\cos\phi,\cos\phi_o) \tag{48}$$

The GSTC or GIBC model for this structure cannot dsicriminate whether the stub at the junction is a perfect electric conductor (PEC) or perfect magnetic conductor (PMC). This information can only be carried by the constant b_{10} and its determination must somehow involve the properties of the junction across its thickness as discussed in a subsequent section. However, since the diffraction coefficient for the junction in Figure 5 is already available [15], b_{10} can be identified. Upon setting $w_s = 0$, we find

$$b_{10}^{\text{no stub}} = jkw\sqrt{\frac{\mu_1}{\epsilon_1}} \tag{49}$$

$$b_{10}^{\text{pec stub}} = \frac{jkw\sqrt{\frac{\mu_1}{\epsilon_1}}}{\frac{jkw}{4\epsilon_1}\left(\sqrt{\epsilon_1\mu_1}-1\right)\left[M_-\left(\sqrt{\epsilon_1\mu_1},\gamma_1^{even,1}\right)M_-\left(\sqrt{\epsilon_1\mu_1},\gamma_2^{even,1}\right)\right]^2+\frac{1}{2}} \tag{50}$$

$$b_{10}^{\text{pmc stub}} = \frac{jkw\sqrt{\frac{\mu_1}{\epsilon_1}}}{\frac{jkw}{4\epsilon_1}\left(\sqrt{\epsilon_1\mu_1}-1\right)\left[M_-\left(\sqrt{\epsilon_1\mu_1},\gamma_1^{even,1}\right)M_-\left(\sqrt{\epsilon_1\mu_1},\gamma_2^{even,1}\right)\right]^2-\frac{1}{2}} \tag{51}$$

This comparison clearly demonstrates the importance of the constant b_{10} and by referring to Figure 6 we observe that it plays a major role in the computation of the diffracted field.

5 Modal Decomposition of the Symmetric Slab Fields

A general approach for determining the solution constants is to enforce tangential field continuity accross the junction. This, of course, demands a knowledge of the fields internal to the discontinuous slab, which are not readily available when a GSTC simulation is employed. The Weiner-Hopf (or dual integral equations) solution in conjunction with the GSTC provides only the fields external to the slab, and this section deals with the determination of the internal fields from the external ones.

A modal representation of the internal field is first proposed comprised of discrete and continuous spectral components. This representation is compatible with that given by Shevchenko [16] whose eigenfunctions are chosen to satisfy field continuity across all layer interfaces including the air-dielectric interface. Consequently, the representation is valid inside and

outside the dielectric once the coefficients of the modal representation are determined. This is accomplished by recasting the Weiner-Hopf or dual integral equation solution given earlier (see (13), (14), (29) and (33)) in a form compatible with the proposed modal representation, thus permitting the identification of the modal or eigenfunction coefficients. These will, of course, be in terms of the unknown constants appearing in the Weiner-Hopf solution and the enforcement of field continuity across the junction leads to a linear system of equations to be solved for the constants as described in the next section.

For the symmetric slab in Figure 2, the total field may be decomposed into its odd and even components. Specifically we write

$$F(x,y) = \begin{cases} F^{1,odd}(x,y) + F^{1,even}(x,y) & x < 0 \\ \\ F^{2,odd}(x,y) + F^{2,even}(x,y) & x > 0 \end{cases} \tag{52}$$

where $F^{odd}(x,y) = -F^{odd}(x,-y)$ and $F^{even}(x,y) = F^{even}(x,-y)$. Following [16], the odd and even fields interior and exterior to the slab may be expanded into discrete and continuous eigenmodes as

$$\begin{aligned} F^{1,odd}(x,y) &= \sum_{m=1}^{N_{go}} A_m^{1,odd} \Psi^{1,odd}\left(\left(\lambda_m^{1,go}\right)^2, y\right) e^{-jkx\lambda_m^{1,go}} \\ &\quad + \sum_{m=1}^{N_{sw}^{1,odd}} B_m^{1,odd} \Phi_m^{1,odd}(y)\, e^{-jkx\lambda_m^{1,odd}} \\ &\quad + \int_0^{\infty} C^{1,odd}(\beta)\, \Psi^{1,odd}\left(\lambda^2, y\right) e^{-jkx\lambda} d\beta \end{aligned} \tag{53}$$

$$\begin{aligned} F^{1,even}(x,y) &= \sum_{m=1}^{N_{go}} A_m^{1,even} \Psi^{1,even}\left(\left(\lambda_m^{1,go}\right)^2, y\right) e^{-jkx\lambda_m^{1,go}} \\ &\quad + \sum_{m=1}^{N_{sw}^{1,even}} B_m^{1,even} \Phi_m^{1,even}(y)\, e^{-jkx\lambda_m^{1,even}} \\ &\quad + \int_0^{\infty} C^{1,even}(\beta)\, \Psi^{1,even}\left(\lambda^2, y\right) e^{-jkx\lambda} d\beta \end{aligned} \tag{54}$$

$$F^{2,odd}(x,y) = \sum_{m=1}^{N_{go}} A_m^{2,odd} \Psi^{2,odd}\left(\left(\lambda_m^{2,go}\right)^2, y\right) e^{-jkx\lambda_m^{2,go}}$$

$$+\sum_{m=1}^{N_{sw}^{2,odd}} B_m^{2,odd}\Phi_m^{2,odd}(y)\,e^{-jkx\lambda_m^{2,odd}}$$
$$+\int_0^{\infty} C^{2,odd}(\beta)\,\Psi^{2,odd}\left(\lambda^2,y\right)e^{-jkx\lambda}d\beta \qquad (55)$$

$$F^{2,even}(x,y) = \sum_{m=1}^{N_{go}} A_m^{2,even}\Psi^{2,even}\left(\left(\lambda_m^{2,go}\right)^2,y\right)e^{-jkx\lambda_m^{23,go}}$$
$$+\sum_{m=1}^{N_{sw}^{2,even}} B_m^{2,even}\Phi_m^{2,even}(y)\,e^{-jkx\lambda_m^{2,even}}$$
$$+\int_0^{\infty} C^{2,even}(\beta)\,\Psi^{2,even}\left(\lambda^2,y\right)e^{-jkx\lambda}d\beta \qquad (56)$$

where $Im\{\lambda_m^{odd,even}\} < 0$ and $\lambda = \sqrt{1-\beta^2}$, with the branch of the square root chosen so that $Im\{\sqrt{1-\beta^2}\} < 0$. In (53)- (56), $\Psi^{odd,even}$ are referred to as the cross section functions corresponding to the continuous modal fields whereas $\Phi_m^{odd,even}$ are the corresponding cross section functions for the discrete modal fields associated with the surface waves. The cross section function associated with the geometrical optics fields is also $\Psi^{odd,even}$ evaluated at $\lambda = \lambda_m^{go}$, where $\lambda_m^{go}$is a parameter to be determined later. As can be observed from (53) - (56), the cross section functions specify the field behavior in the plane normal to the slab, and hence all information pertaining to the fields interior to the slab are embedded into these functions. They will be chosen to satisfy the orthogonality relations (where $u(y)$ is $\mu(y)$ or $\epsilon(y)$ for E_z or H_z polarization, respectively)

$$\int_{-\infty}^{\infty} \frac{\Psi(\lambda^2,y)\,\Psi\left(\tilde{\lambda}^2,y\right)}{u(y)}dy = 0 \quad \text{for } \lambda \neq \tilde{\lambda} \qquad (57)$$

$$\int_{-\infty}^{\infty} \frac{\Phi_m(y)\,\Psi(\lambda^2,y)}{u(y)}dy = 0 \qquad (58)$$

and thus each discrete eigenmode $\Phi_m(y)\,e^{-jkx\lambda}$ and each continuous eigenmode $\Psi(\lambda^2,y)\,e^{-jkx\lambda}$ must satisfy the wave equation. Additional details pertaining to the cross section functions are given in [16].

Exterior Cross Section Functions

To compute the cross section functions in the exterior slab region $|y| > \tau/2$, we recall that in accordance with the slab simulation based on the generalized sheet transition conditions (GSTCs), the external fields satisfy the conditions (10) and (11). Because of the orthogonality relations (57) and (58), each of the cross section functions $\Psi(\lambda^2, y)$ and $\Phi_m(y)$ must then satisfy their respective odd or even GSTC. In view of this we set

$$\begin{aligned}\Psi^{p,odd}\left(\lambda^2, y\right) &= \frac{|y|}{y}\left\{\mathcal{U}_{11}^{p}\left(\lambda^2\right) j\frac{\sin\left[k\left(|y|-\tau/2\right)\sqrt{1-\lambda^2}\right]}{\sqrt{1-\lambda^2}}\right. \\ &\quad \left.+\mathcal{U}_{12}^{p}\left(\lambda^2\right)\cos\left[k\left(|y|-\tau/2\right)\sqrt{1-\lambda^2}\right]\right\} \\ &= \frac{|y|}{y}\left\{\mathcal{U}_{11}^{p}\left(\lambda^2\right)\tilde{q}_{12}(1,1,|y|-\tau/2,\lambda^2)\right. \\ &\quad \left.+\mathcal{U}_{12}^{p}\left(\lambda^2\right)\tilde{q}_{22}(1,1,|y|-\tau/2,\lambda^2)\right\} \qquad (59)\end{aligned}$$

$$\begin{aligned}\Psi^{p,even}\left(\lambda^2, y\right) &= \left\{\mathcal{U}_{21}^{p}\left(\lambda^2\right) j\frac{\sin\left[k\left(|y|-\tau/2\right)\sqrt{1-\lambda^2}\right]}{\sqrt{1-\lambda^2}}\right. \\ &\quad \left.+\mathcal{U}_{22}^{p}\left(\lambda^2\right)\cos\left[k\left(|y|-\tau/2\right)\sqrt{1-\lambda^2}\right]\right\} \\ &= \left\{\mathcal{U}_{21}^{p}\left(\lambda^2\right)\tilde{q}_{12}(1,1,|y|-\tau/2,\lambda^2)\right. \\ &\quad \left.+\mathcal{U}_{22}^{p}\left(\lambda^2\right)\tilde{q}_{22}(1,1,|y|-\tau/2,\lambda^2)\right\} \qquad (60)\end{aligned}$$

where $\tilde{q}_{ij}$ represents the infinite order form of the q_{ij} layer operators given in [10]. Once each of the modes comprising (53) through (56) is substituted into (10) or (11), the differentiation implied by $-\partial x^2/k^2$ reduces to a multiplication by λ^2 and the above $\Psi^{p,odd}$ and $\Psi^{p,even}$ are then readily shown to satisfy the associated GSTC. It can also be shown that these satisfy the orthogonality conditions (57) and (58).

A customary representation for the surface wave cross section functions is

$$\Phi_m^{p,odd}(y) = \frac{|y|}{y}e^{-jk(|y|-\tau/2)\sqrt{1-\left(\lambda_m^{p,odd}\right)^2}} \quad ;|y|>\tau/2 \qquad (61)$$

$$\Phi_m^{p,even}(y) = e^{-jk(|y|-\tau/2)\sqrt{1-\left(\lambda_m^{p,even}\right)^2}} \quad ;|y|>\tau/2 \qquad (62)$$

where $\lambda_m^{p,even,odd}$ must now be chosen so that they satisfy their associated GSTC. By substituting (61) and (62) into (10) and (11), we find that $\lambda_m^{odd,even}$ must satisfy the polynomial equations

$$\sqrt{1-\left(\lambda_m^{p,odd}\right)^2}\mathcal{U}_{12}^p\left(\left[\lambda_m^{p,odd}\right]^2\right)+\mathcal{U}_{11}^p\left(\left[\lambda_m^{p,odd}\right]^2\right) = 0 \qquad (63)$$

$$\sqrt{1-(\lambda_m^{p,even})^2}\mathcal{U}_{22}^p\left([\lambda_m^{p,even}]^2\right)+\mathcal{U}_{21}^p\left([\lambda_m^{p,even}]^2\right) = 0 \qquad (64)$$

and can be also identified as the poles of the slab plane wave reflection coefficient. We further note that

$$\Phi_m^{p,odd}(y) = \frac{\Psi^{p,odd}\left(\left[\lambda_m^{p,odd}\right]^2,y\right)}{\mathcal{U}_{12}^p\left(\left[\lambda_m^{p,odd}\right]^2\right)}; \quad |y|>\tau/2 \qquad (65)$$

$$\Phi_m^{p,even}(y) = \frac{\Psi^{p,even}\left([\lambda_m^{p,even}]^2,y\right)}{\mathcal{U}_{22}^p\left([\lambda_m^{p,even}]^2\right)}; \quad |y|>\tau/2 \qquad (66)$$

implying that for a multilayer slab the cross section functions associated with the discrete and continuous eigenmodes are of the same generic form given by (59) and (60).

Interior Cross Section Functions

We consider now the determination of the cross section functions for the region interior to the slab (i.e. in the region $|y|<\tau/2$). For simplicity let us first assume a single layer slab of thickness $\tau=\tau_1$, whose upper face is located at $y=-\tau_1/2$. In accordance with the preceeding, the cross section functions associated with the external fields are given by

$$\Psi^{p,odd}\left(\lambda^2,y\right) = \frac{|y|}{y}\Big\{q_{11}\left(u_1^p,\kappa_1^p,\tau_1^p,\lambda^2\right)\tilde{q}_{12}(1,1,|y|-\tau_1/2,\lambda^2) + q_{12}\left(u_1^p,\kappa_1^p,\tau_1^p,\lambda^2\right)\tilde{q}_{22}(1,1,|y|-\tau_1/2,\lambda^2)\Big\}; \quad |y|>\tau_1/2 \qquad (67)$$

$$\Psi^{p,even}\left(\lambda^2,y\right) = \Big\{q_{21}\left(u_1^p,\kappa_1^p,\tau_1^p,\lambda^2\right)\tilde{q}_{12}(1,1,|y|-\tau_1/2,\lambda^2) + q_{22}\left(u_1^p,\kappa_1^p,\tau_1^p,\lambda^2\right)\tilde{q}_{22}(1,1,|y|-\tau_1/2,\lambda^2)\Big\}; \quad |y|>\tau_1/2 \qquad (68)$$

obtained by setting $\mathcal{U}_{ij}^{p}(\lambda^2) = q_{ij}(u_1^p, \kappa_1^p, \tau_1^p, \lambda^2)$ in (59) and (60). These are orthogonal functions and each must, therefore, satisfy the continuity conditions

$$\Psi^{p,odd}\left(\lambda^2, \tau_1^-\right) = \Psi^{p,odd}\left(\lambda^2, \tau_1^+\right) \tag{69}$$

$$\frac{1}{u_1}\partial y \Psi^{p,odd}\left(\lambda^2, \tau_1^-\right) = \partial y \Psi^{p,odd}\left(\lambda^2, \tau_1^+\right) \tag{70}$$

$$\Psi^{p,even}\left(\lambda^2, \tau_1^-\right) = \Psi^{p,even}\left(\lambda^2, \tau_1^+\right) \tag{71}$$

$$\frac{1}{u_1}\partial y \Psi^{p,even}\left(\lambda^2, \tau_1^-\right) = \partial y \Psi^{p,even}\left(\lambda^2, \tau_1^+\right) \tag{72}$$

with similar conditions on $\Phi_m^{odd,even}(y)$. It is now straightforward to deduce that possible cross section functions satisfying (69) - (72) are of the form

$$\Psi^{p,odd}\left(\lambda^2, y\right) = \frac{|y|}{y} q_{12}(u_1^p, \kappa_1^p, |y|, \lambda^2) \tag{73}$$

$$\Psi^{p,even}\left(\lambda^2, y\right) = q_{22}(u_1^p, \kappa_1^p, |y|, \lambda^2) \tag{74}$$

for $|y| < \tau/2$. Also, in view of (69) - (72), the cross section functions for the surface wave modes remain as given in (65) - (66), provided (73) and (74) are used in place of $\Psi^{odd,even}$.

For the general case of a multilayer slab, it is necessary that each of the internal cross sections functions satisfy the continuity conditions at all layer interfaces comprising the slab. In this case we find that

$$\Psi^{p,odd}\left(\lambda^2, y\right) = \frac{|y|}{y}\begin{cases} \mathcal{U}_{11}^{p}(\lambda^2)\,\tilde{q}_{12}(1,1,|y|-\tau/2,\lambda^2) \\ \quad +\mathcal{U}_{12}^{p}(\lambda^2)\,\tilde{q}_{22}(1,1,|y|-\tau/2,\lambda^2); \\ \qquad\qquad |y| > \tau/2 \\ \mathcal{P}_{11}^{l,p}(\lambda^2)\,q_{12}(u_l^p, \kappa_l^p, |y|-y_{l-1}, \lambda^2) \\ \quad +\mathcal{P}_{12}^{l,p}(\lambda^2)\,q_{22}(u_l^p, \kappa_l^p, |y|-y_{l-1}, \lambda^2); \\ \qquad\qquad y_l > |y| > y_{l-1} \\ q_{12}(u_1^p, \kappa_1^p, |y|, \lambda^2); \quad |y| < y_1 \end{cases} \tag{75}$$

$$\Psi^{p,even}\left(\lambda^2,y\right) = \begin{cases} \mathcal{U}_{21}^{p}\left(\lambda^2\right)\tilde{q}_{12}(1,1,|y|-\tau/2,\lambda^2) \\ \quad +\mathcal{U}_{22}^{p}\left(\lambda^2\right)\tilde{q}_{22}(1,1,|y|-\tau/2,\lambda^2); \\ \qquad\qquad |y|>\tau/2 \\ \mathcal{P}_{21}^{l,p}\left(\lambda^2\right)q_{12}(u_l^p,\kappa_l^p,|y|-y_{l-1},\lambda^2) \\ \quad +\mathcal{P}_{22}^{l,p}\left(\lambda^2\right)q_{22}(u_l^p,\kappa_l^p,|y|-y_{l-1},\lambda^2); \\ \qquad\qquad y_l>|y|>y_{l-1} \\ q_{22}(u_1^p,\kappa_1^p,|y|,\lambda^2); \quad |y|<y_1 \end{cases} \tag{76}$$

where

$$\begin{bmatrix} \mathcal{P}_{11}^{l,p}\left(-\frac{\partial x^2}{k^2}\right) & \mathcal{P}_{12}^{l,p}\left(-\frac{\partial x^2}{k^2}\right) \\ \mathcal{P}_{21}^{l,p}\left(-\frac{\partial x^2}{k^2}\right) & \mathcal{P}_{22}^{l,p}\left(-\frac{\partial x^2}{k^2}\right) \end{bmatrix} = \prod_{m=1}^{l} \cdot \begin{bmatrix} q_{11}(u_m^p,\kappa_m^p,\tau_m^p,-\frac{\partial x^2}{k^2}) & q_{12}(u_m^p,\kappa_m^p,\tau_m^p,-\frac{\partial x^2}{k^2}) \\ q_{21}(u_m^p,\kappa_m^p,\tau_m^p,-\frac{\partial x^2}{k^2}) & q_{22}(u_m^p,\kappa_m^p,\tau_m^p,-\frac{\partial x^2}{k^2}) \end{bmatrix} \tag{77}$$

When these are used in (53) - (56) in conjunction with (65) and (66) we have a complete field representation for all x.

6 Recasting of the Dual Integral Equation Solution for a Material Junction

The expressions (53) - (56) can be used to represent the fields interior and exterior to the slab. It remains to find the coefficients of these expansions and to do this we must first rewrite $F(x,y)$ in a form compatible with (53) - (56). That is, we need to identify from (13) and (14) the discrete and continuous spectral components. The discrete portion of the spectrum is, of course, comprised of the geometrical optics and the surface wave fields. These can be identified by detouring the integration path in (14) as shown in Figure 7. In particular, for $x<0$ the integration path may be deformed to one over the branch cut in the upper half of the λ plane, capturing any surface wave poles attributed to the zeros of $\mathcal{G}_{1-}^{odd}(\lambda)$ and $\mathcal{G}_{1-}^{even}(\lambda)$. Similarly, for $x>0$, the integration path may be deformed to one over the branch cut in the lower half of the λ plane causing the capture of the geometrical optics pole at $\lambda=-\lambda_o$ in addition to any surface wave poles attributed to the zeros of $\mathcal{G}_{2+}^{odd}(\lambda)$ and $\mathcal{G}_{2+}^{even}(\lambda)$.

Through the above deformation of the integration paths in (14) we obtain

$$F^{odd}(x,y) = \begin{cases} F_{go}^{1,odd}(x,y) + F_{sw}^{1,odd}(x,y) + F_{diff}^{1,odd}(x,y) & x < 0 \\ F_{go}^{2,odd}(x,y) + F_{sw}^{2,odd}(x,y) + F_{diff}^{2,odd}(x,y) & x > 0 \end{cases} \tag{78}$$

$$F^{even}(x,y) = \begin{cases} F_{go}^{1,even}(x,y) + F_{sw}^{1,even}(x,y) + F_{diff}^{1,even}(x,y) & x < 0 \\ F_{go}^{2,even}(x,y) + F_{sw}^{2,even}(x,y) + F_{diff}^{2,even}(x,y) & x > 0 \end{cases} \tag{79}$$

where the components F_{go}, F_{sw}, F_{diff} denote the geometrical optics, surface wave, and branch cut (or diffraction) contributions to the total fields.

After some manipulation we find

$$F_{go}^{1,odd}(x,y) = A_1^{1,odd}(\lambda_o)\,\Psi^{1,odd}\left(\lambda_o^2, y\right) e^{jkx\cos\phi_o} \tag{80}$$

$$F_{go}^{2,odd}(x,y) = A_1^{2,odd}(\lambda_o)\,\Psi^{2,odd}\left(\lambda_o^2, y\right) e^{jkx\cos\phi_o} \tag{81}$$

$$F_{go}^{1,even}(x,y) = A_1^{1,even}(\lambda_o)\,\Psi^{1,even}\left(\lambda_o^2, y\right) e^{jkx\cos\phi_o} \tag{82}$$

$$F_{go}^{2,even}(x,y) = A_1^{2,even}(\lambda_o)\,\Psi^{2,even}\left(\lambda_o^2, y\right) e^{jkx\cos\phi_o} \tag{83}$$

where the A expansion coefficients are identified as

$$A_1^{1,odd}(\lambda_o) = \frac{\sin\phi_o e^{jk\tau/2\sin\phi_o}}{\mathcal{G}_1^{odd}(\lambda_o^2)} \tag{84}$$

$$A_1^{2,odd}(\lambda_o) = \frac{\sin\phi_o e^{jk\tau/2\sin\phi_o}}{\mathcal{G}_2^{odd}(\lambda_o^2)} \tag{85}$$

$$A_1^{1,even}(\lambda_o) = \frac{\sin\phi_o e^{jk\tau/2\sin\phi_o}}{\mathcal{G}_1^{even}(\lambda_o^2)} \tag{86}$$

$$A_1^{2,even}(\lambda_o) = \frac{\sin\phi_o e^{jk\tau/2\sin\phi_o}}{\mathcal{G}_2^{even}(\lambda_o^2)} \tag{87}$$

For the B coefficients, we have

$$F_{sw}^{1,odd}(x,y) = \sum_{l=1}^{N_{sw}^{1,odd}} B_l^{1,odd}(\lambda_o)\left[Z_{odd}\left(-\lambda_o\lambda_l^{1,odd}\right)\right.$$

$$+\sum_{m=1}^{\tilde{N}_{odd}-1}\sum_{n=0}^{\tilde{N}_{odd}-1-m} a_{mn}\left(\lambda_l^{1,odd}+\lambda_o\right)^m\left(\lambda_l^{1,odd}\lambda_o\right)^n\Bigg]$$
$$\cdot\,\Psi^{1,odd}\left(\left[\lambda_l^{1,odd}\right]^2,y\right)e^{-jkx\lambda_l^{1,odd}} \tag{88}$$

$$F_{sw}^{1,even}(x,y) = \sum_{l=1}^{N_{sw}^{1,even}} B_l^{1,even}(\lambda_o)\Bigg[Z_{odd}\left(-\lambda_o\lambda_l^{1,even}\right)$$
$$+\sum_{m=1}^{\tilde{N}_{even}-1}\sum_{n=0}^{\tilde{N}_{even}-1-m} b_{mn}\left(\lambda_l^{1,even}+\lambda_o\right)^m\left(\lambda_l^{1,even}\lambda_o\right)^n\Bigg]$$
$$\cdot\,\Psi^{1,even}\left(\left[\lambda_l^{1,even}\right]^2,y\right)e^{-jkx\lambda_l^{1,even}} \tag{89}$$

with

$$B_l^{1,odd}(\lambda_o) = \frac{-\sin\phi_o}{\lambda_l^{1,odd}+\lambda_o}$$
$$\cdot\,\frac{e^{jk\tau/2\sin\phi_o}}{\left[\frac{\partial\mathcal{G}_{1-}^{odd}(\lambda)}{\partial\lambda}\right]_{\lambda=\lambda_l^{1,odd}}\mathcal{G}_{1-}^{odd}(\lambda_o)\,\mathcal{G}_{2+}^{odd}\left(\lambda_l^{1,odd}\right)\mathcal{G}_{2+}^{odd}(\lambda_o)} \tag{90}$$

$$B_l^{1,even}(\lambda_o) = \frac{-\sin\phi_o}{\lambda_l^{1,even}+\lambda_o}$$
$$\cdot\,\frac{e^{jk\tau/2\sin\phi_o}}{\left[\frac{\partial\mathcal{G}_{1-}^{even}(\lambda)}{\partial\lambda}\right]_{\lambda=\lambda_l^{1,even}}\mathcal{G}_{1-}^{even}(\lambda_o)\,\mathcal{G}_{2+}^{even}\left(\lambda_l^{1,even}\right)\mathcal{G}_{2+}^{even}(\lambda_o)} \tag{91}$$

The expressions for $F_{sw}^{2,odd}(x,y)$ and $F_{sw}^{2,even}(x,y)$ parallel those in (86) and (87).

To obtain the C coefficient we express $F_{diff}^{1,odd}$ as

$$F_{diff}^{1,odd}(x,y) = \frac{y}{|y|}\int_{-\infty}^{\infty}\frac{j}{2\pi}\frac{-\beta\sqrt{1-\lambda_o^2}}{\sqrt{1-\beta^2}\left(\sqrt{1-\beta^2}+\lambda_o\right)}$$
$$\cdot\,\frac{e^{jk\tau/2\left(\sqrt{1-\lambda_o^2}+\beta\right)}e^{-jk|y|\beta}e^{-jkx\sqrt{1-\beta^2}}}{\mathcal{G}_{1-}^{odd}\left(\sqrt{1-\beta^2}+\delta\frac{\beta}{|\beta|}\right)\mathcal{G}_{1-}^{odd}(\lambda_o)\,\mathcal{G}_{2+}^{odd}\left(\sqrt{1-\beta^2}\right)\mathcal{G}_{2+}^{odd}(\lambda_o)}$$

$$\cdot\left[Z_{odd}\left(-\lambda_o\sqrt{1-\beta^2}\right)+\sum_{m=1}^{\widetilde{N}_{odd}-1}\sum_{n=0}^{\widetilde{N}_{odd}-1-m}\right.$$

$$\left.\cdot a_{mn}\left(\lambda_o+\sqrt{1-\beta^2}\right)^m\left(\lambda_o\sqrt{1-\beta^2}\right)^n\right]d\beta \qquad (92)$$

where the branch of the square root is chosen so that $Im\left(\sqrt{1-\beta^2}\right)>0$ and δ is a vanishingly small positive number. By splitting the integral into its positive and negative portions, and employing some identities (92) becomes

$$F_{diff}^{1,odd}(x,y) = \int_0^\infty C^{1,odd}(\beta)\,\tilde{Z}_{odd}\left(\sqrt{1-\beta^2},\lambda_o\right)$$

$$\cdot\,\Psi^{1,odd}\left(1-\beta^2,y\right)e^{-jkx\sqrt{1-\beta^2}}d\beta \qquad (93)$$

with the expansion coefficient $C^{1,odd}(\beta)$ given by

$$C^{1,odd}(\beta)=\frac{j}{\pi}\frac{\beta^2\sqrt{1-\lambda_o^2}}{\sqrt{1-\beta^2}\left(\sqrt{1-\beta^2}+\lambda_o\right)}$$

$$\cdot\frac{e^{jk\tau/2\sqrt{1-\lambda_o^2}}\mathcal{G}_{1+}^{odd}\left(\sqrt{1-\beta^2}\right)}{\mathcal{G}_{2+}^{odd}\left(\sqrt{1-\beta^2}\right)\mathcal{G}_{2+}^{odd}(\lambda_o)\,\mathcal{G}_{1-}^{odd}(\lambda_o)\left\{\left[\mathcal{U}_{11}^1\left(1-\beta^2\right)\right]^2-\beta^2\left[\mathcal{U}_{12}^1\left(1-\beta^2\right)\right]^2\right\}} \qquad (94)$$

Similar expressions for $F_{diff}^{2,odd}(x,y)$, $F_{diff}^{1,even}(x,y)$ and $F_{diff}^{2,even}$ can be obtained in a parallel manner leading to the identification of the remaining C coefficient.

7 Determination of the Constants

To determine the constants a_{mn} and b_{mn}, we may now enforce the tangential field continuity conditions

$$F\left(x=0^-,y\right)=F\left(x=0^+,y\right);\quad |y|<\tau/2 \qquad (95)$$

$$\frac{1}{u_1(y)}\partial xF(x,y)_{x=0^-}=\frac{1}{u_2(y)}\partial xF(x,y)_{x=0^+};\quad |y|<\tau/2 \qquad (96)$$

with

$$u_{1,2}(y) = \begin{cases} \mu_{1,2}(y) & E_z\text{-pol} \\ \epsilon_{1,2}(y) & H_z\text{-pol} \end{cases} \tag{97}$$

and the subscripts 1 and 2 denoting quantities attributed to the left and right side of the slab. Substituting (79) - (79) into (95) and (96), we obtain

$$\begin{aligned} &F_{go}^{1,odd}\left(x=0^-,y\right)+F_{sw}^{1,odd}\left(x=0^-,y\right)+F_{diff}^{1,odd}\left(x=0^-,y\right) \\ &\quad=F_{go}^{2,odd}\left(x=0^+,y\right)+F_{sw}^{2,odd}\left(x=0^+,y\right)+F_{diff}^{2,odd}\left(x=0^+,y\right) \end{aligned} \tag{98}$$

$$\begin{aligned} &\frac{1}{u_1(y)}\partial x\left[F_{go}^{1,odd}(x,y)+F_{sw}^{1,odd}(x,y)+F_{diff}^{1,odd}(x,y)\right]_{x=0^-} \\ &\quad=\frac{1}{u_2(y)}\partial x\left[F_{go}^{2,odd}(x,y)+F_{sw}^{2,odd}(x,y)+F_{diff}^{2,odd}(x,y)\right]_{x=0^+} \end{aligned} \tag{99}$$

$$\begin{aligned} &F_{go}^{1,even}\left(x=0^-,y\right)+F_{sw}^{1,even}\left(x=0^-,y\right)+F_{diff}^{1,even}\left(x=0^-,y\right) \\ &\quad=F_{go}^{2,even}\left(x=0^+,y\right)+F_{sw}^{2,even}\left(x=0^+,y\right)+F_{diff}^{2,even}\left(x=0^+,y\right) \end{aligned} \tag{100}$$

$$\begin{aligned} &\frac{1}{u_1(y)}\partial x\left[F_{go}^{1,even}(x,y)+F_{sw}^{1,even}(x,y)+F_{diff}^{1,even}(x,y)\right]_{x=0^-} \\ &\quad=\frac{1}{u_2(y)}\partial x\left[F_{go}^{2,even}(x,y)+F_{sw}^{2,even}(x,y)+F_{diff}^{2,even}(x,y)\right]_{x=0^+} \end{aligned} \tag{101}$$

to be solved for all a_{mn} and b_{mn}. In particular, for an odd GSTC of $O(N_1^{odd})$ to the left and of $O(N_2^{odd})$ to the right of the discontinuity, the number of a_{mn} to be determined is equal to

$$\begin{aligned} N_a &= \frac{\widetilde{N}_{odd}\left(\widetilde{N}_{odd}-1\right)}{2} \\ &= \begin{cases} \frac{\left(N_{odd}^1+N_{odd}^2\right)\left(N_{odd}^1+N_{odd}^2-2\right)}{8}; & N_{odd}^1+N_{odd}^2 \text{ is even} \\ \frac{\left(N_{odd}^1+N_{odd}^2\right)^2-1}{8}; & N_{odd}^1+N_{odd}^2 \text{ is odd} \end{cases} \end{aligned} \tag{102}$$

To determine all a constants, (99) and/or (100) must then be enforced or sampled at a minimum of N_a points accross $|y| < \tau/2$ and $0 < \phi_o < \pi$. Similarly for an even GSTC of $O(N_1^{even})$ to the left and of $O(N_2^{even})$ to the

right of the discontinuity,

$$\begin{aligned} N_b &= \frac{\widetilde{N}_{even}\left(\widetilde{N}_{even}-1\right)}{2} \\ &= \begin{cases} \frac{\left(N^1_{even}+N^2_{even}\right)\left(N^1_{even}+N^2_{even}-2\right)}{8}; & N^1_{even}+N^2_{even} \text{ is even} \\ \frac{\left(N^1_{even}+N^2_{even}\right)^2-1}{8}; & N^1_{even}+N^2_{even} \text{ is odd} \end{cases} \end{aligned} \tag{103}$$

and thus, the b constants can be determined by enforcing (101) and/or (101) at a minimum of N_b points.

Substituting for the fields in (99) and (100) as given in the previous section, we obtain the equations

$$V_F^{odd}(\lambda_o, y) = \sum_{p=1}^{N_a} a_p Z_F^{odd}(m(p), n(p), \lambda_o, y) \tag{104}$$

$$V_{\partial xF}^{odd}(\lambda_o, y) = \sum_{p=1}^{N_a} a_p Z_{\partial xF}^{odd}(m(p), n(p), \lambda_o, y) \tag{105}$$

where $a_p = a_{m(p)n(p)}$ with

$$p = \frac{(n+m-1)(m+n)}{2} + m \tag{106}$$

$$\begin{aligned} m(p) &= p - \frac{1}{2} Int\left\{\frac{\sqrt{1+8(p-1)}-1}{2}\right\} \\ &\quad \cdot Int\left\{\frac{\sqrt{1+8(p-1)}+1}{2}\right\} \end{aligned} \tag{107}$$

$$n(p) = Int\left\{\frac{\sqrt{1+8(p-1)}+1}{2}\right\} - m(p) \tag{108}$$

which are in accordance with the ordering of the a_{mn} constants as the order of the GSTC is increased (see Figure 8). The functions V_F^{odd}, $V_{\partial xF}^{odd}$, Z_F^{odd} and $Z_{\partial xF}^{odd}$ are readily determined from the previous analysis and are not quoted here.

Equations similar to (104) - (105) can be obtained for the b constants in a parallel manner.

8 Validation of the Solution

The validity of the derived angular spectra and diffraction coefficients was already performed to a limited degree in Section 4 of the paper. What remains, therefore, is a validation of the procedure for computing the constants a_{mn} and b_{mn} which amounts to solving a small matrix. The validation was done by comparison with processed data from a numerical model which consisted of a finite length slab having the prescribed discontinuity or junction at its center. First, the transient response of this finite slab was generated from bandlimited frequency domain data. The contribution from the material junction was then obtained by time gating the transient response. Numerically derived data from this procedure were found in good agreement with the presented analytical solution. An example is shown in Figure 9 corresponding to a thick (0.2 freespace wavelengths) material half plane. The numerical and analytical data are clearly in good agreement, and it is again demonstrated that the constants play a major role in the solution.

9 Other Applications of the GIBC/GSTC

It was shown above that the GIBC can effectively model thick planar layers of material. However, corresponding GIBC can also be derived for curved coated surfaces (see Figure 10), and the improved accuracy of these is particularly evident when surface wave effects are dominant. For surfaces having relatively large radii of curvature these can be easily derived from those of the planar surface with x and z replaced by the local tangential variables and y by the normal one. With a second order GIBC derived in this manner, the Mie series and GTD solutions have been found [20], [21] and compared with the exact modal series solution for a coated cylinder. As illustrated in Figure 11, the field given by the Mie series based on the GIBC is in excellent agreement with the exact result even at points close to the surface in the shadow region where a finite order boundary condition is inadequate. In contrast, data based on the standard impedance boundary condition (SIBC) are substantially inaccurate.

Higher order boundary conditions have advantages in numerical treat-

ments as well. When used to simulate a coating, a GIBC eliminates the need to sample inside the dielectric, and this is important when storage is limited. In addition, it may be possible to use a GIBC to transfer a boundary condition to a plane, thereby producing a boundary integral equation of convolution type. In conjunction with an FFT, the equation can be solved iteratively to reduce the storage requirement to $O(n)$ where n is the number of unknowns. As an example, for the three dimensional problem of a cavity in a coated ground plane, a GIBC provides a simple modal as well as a reduction in memory. If the coating is lossy or tapered in thickness, the non-uniqueness due to the terminations is avoided, and the same is true for cavities whose depth tapers to zero. Nevertheless, caution must be exercised when solving the integral equation numerically. The GIBC results in higher order derivatives applied to the Green's function, and even if some can be transferred to the current, the increased singularity of the Green's function makes discretization more difficult. In spite of this, integral equation methods using GIBCs of up to the third oder have been successfully implemented [22].

Appendix: Multiplicative Split Functions

In this appendix we consider the splitting of

$$\mathcal{G}\left(\lambda^2\right) = \mathcal{U}_A\left(\lambda^2\right) + \sqrt{1-\lambda^2}\mathcal{U}_B\left(\lambda^2\right) \tag{109}$$

as a product of two functions, one of which is free of poles, zeros and branch cuts in the upper half of the λ plane and the other having the same properties in the lower half of the λ plane. That is, we seek to write $\mathcal{G}\left(\lambda^2\right)$ in the form

$$\mathcal{G}\left(\lambda^2\right) = \mathcal{G}_+\left(\lambda\right)\mathcal{G}_-\left(\lambda\right) \tag{110}$$

where the superscript + and - indicate an upper or lower function, respectively. Noting that

$$\mathcal{U}_A\left(\lambda^2\right) = \sum_{n=0}^{N_A} A_n\left[1-\lambda^2\right]^n \tag{111}$$

$$\mathcal{U}_B\left(\lambda^2\right) = \sum_{n=0}^{N_B} B_n\left[1-\lambda^2\right]^n \tag{112}$$

with $N_A = N_B$ or $N_A = N_B + 1$, we may rewrite $\mathcal{G}\left(\lambda^2\right)$ as

$$\mathcal{G}\left(\lambda^2\right) = \sum_{n=0}^{N_S} S_n\left[\sqrt{1-\lambda^2}\right]^n \tag{113}$$

where $N_s = Max(2N_A, 2N_B+1)$ and $S_n = A_{n/2}$ if n is even and $S_n = B_{(n-1)/2}$ if n is odd. However, since we seek a multiplicative splitting of (113), a more convenient form to represent $\mathcal{G}\left(\lambda^2\right)$ is

$$\mathcal{G}\left(\lambda^2\right) = S_0\prod_{n=1}^{N_S}\left(1+\frac{\sqrt{1-\lambda^2}}{\gamma_n}\right) \tag{114}$$

in which γ_n denote the zeros of the polynomial $\sum_{l=0}^{N_S} S_l\left(-\lambda\right)^l$. We immediately now identify that each of the product terms in (114) can be factored as

$$1+\frac{\sqrt{1-\lambda^2}}{\gamma} \stackrel{def}{=} M_+\left(\lambda;\gamma\right)M_-\left(\lambda;\gamma\right) \tag{115}$$

where

$$K_+(\lambda;1/\gamma) = \frac{\sqrt{1-\lambda}}{M_+(\lambda;\gamma)} \tag{116}$$

is the split function characteristic to the impedance half plane having a constant surface impedance $1/\gamma$ [17]. With the branch choosen so that $Im(\sqrt{1-\lambda^2}) < 0$, $M_+(\lambda;\gamma)$ is explicitly given by

$$M_+(\lambda;\gamma) = M_-(-\lambda;\gamma) = \begin{cases} \widetilde{M}_+(\lambda;\gamma) & Im(\gamma) \le 0 \\ \frac{j\eta\left(\lambda-\sqrt{1-\gamma^2}\right)}{\widetilde{M}_+(\lambda;-\gamma)} & Im(\gamma) > 0, \end{cases} \tag{117}$$

$$\widetilde{M}_+(\cos\alpha;1/\eta) = \frac{\Psi_\pi^4(\pi/2)\left[1+\sqrt{2}\cos\left(\frac{\pi/2-\alpha+\theta}{2}\right)\right]\left[1+\sqrt{2}\cos\left(\frac{3\pi/2-\alpha-\theta}{2}\right)\right]}{\sqrt{\frac{8}{\eta}}\left[\Psi_\pi(3\pi/2-\alpha-\theta)\,\Psi_\pi(\pi/2-\alpha+\theta)\right]^2} \tag{118}$$

In this,

$$\begin{aligned} Im(\eta) &\ge 0 \\ \lambda &= \cos\alpha \\ Im\left(\sqrt{1-1/\eta^2}\right) &\le 0 \\ \theta &= \sin^{-1}(\eta) \text{ with } 0 \le Re(\theta), \end{aligned} \tag{119}$$

and $\Psi_\pi(\alpha)$ is the Maliuzhinets function [18] whose evaluation in algebraic form has been given in [19].

The determination of $\mathcal{G}_\pm(\lambda)$ is now rather trivial. By substituting (115) into (114) we easily obtain

$$\mathcal{G}_+(\lambda) = \mathcal{G}_-(-\lambda) = \sqrt{S_0}\prod_{n=1}^{N_S} M_+(\lambda;\gamma_n) \tag{120}$$

References

[1] T. B. A. Senior, "Impedance Boundary Conditions for Imperfectly Conducting Surfaces," *Appl. Sci. Res.*, Vol. 8(B), pp.418-436, 1960.

[2] T. B. A. Senior, "Combined Resistive and Conductive Sheets," *IEEE Trans. on Antennas and Propagat.*, AP-33, No. 5, pp. 577-579, May 1985.

[3] J. Kane and S. N. Karp, "An Accurate Boundary Condition to Replace Transition Condition at Dielectric-Dielectric Interfaces," Institute of Mathematical Sciences Division of E.M. Research, New York University, New York, N. Y., Research Report EM-153, May 1960a.

[4] S. N. Karp and F. C. Karal Jr., "Generalized Impedance Boundary Conditions with Applications to Surface Wave Structures," in Electromagnetic Wave Theory, Part 1, ed. J. Brown, pp. 479-483, Pergamon: New York, 1965.

[5] L. A. Weinstein, The Theory of Diffraction and the Factorization Method, Golem Press: Boulder, CO., 1969.

[6] T. B. A. Senior and J. L. Volakis, "Sheet Simulation of a Thin Dielectric Layer," *Radio Science*, vol. 22, pp. 1261-1271, December 1987.

[7] J. M. L. Bernard, "Diffraction by Metallic Wedge Covered with a Dielectric Material," *Journal of Wave Motion*, Vol. 9, pp. 543-561, 1987.

[8] R. G. Rojas, and Z. Al-hekail, "Generalized Impedance/Resistive Boundary Conditions for Electromagnetic Scattering Problems," *Radio Science*, Vol. 24, No. 1, pp. 1-12, Jan-Feb 1989.

[9] T. B. A. Senior and J. L. Volakis, "Derivation and Application of a Class of Generalized Boundary Conditions," *IEEE Trans. on Antennas and Propagat.*, AP-37, No. 12, December, 1989.

[10] M. A. Ricoy and J. L. Volakis, "Derivation of generalized transition/boundary conditions for planar multiple layer structures," *Radio Science* (in press).

[11] J. L. Volakis, and T. B. A. Senior, "Application of a Class of Generalized Boundary Conditions to Scattering by a Metal-Backed Dielectric Half Plane," *Proceedings of the IEEE*, pp 796-805, May 1989.

[12] T. B. A. Senior, "Diffraction by a Generalized Impedance Half Plane," presented at URSI International Electromagnetic Wave Theory Symposium, Stockholm, Sweden, 14-17 August 1989.

[13] P. C. Clemmow, "A method for the exact solution of a class of two-dimensional diffraction problems," *Proc. Roy. Soc. A*, Vol. 205, pp. 286-308, 1951.

[14] J. L. Volakis, and M. A. Ricoy, "Diffraction by a thick perfectly conducting half-plane," *IEEE Trans. on Antennas and Propagat.*, AP-35, No. 1, pp. 62-72, January, 1987.

[15] M. A. Ricoy and J. L. Volakis, "Diffraction by a Multilayer Slab Recessed in a Ground Plane via Generalized Impedance Boundary Conditions," submitted to *Radio Science.*

[16] V. V. Shevchenko, Continuous Transitions in Open Waveguides, Golem Press: Boulder, CO., 1971.

[17] T. B. A. Senior, "Diffraction by a semi-infinite metallic sheet, *Proc. Roy. Soc.* (London), A213,pp. 436-458, 1952.

[18] G.D. Maliuzhinets, " Excitation, Reflection and Emission Of Surface Waves From a Wedge With Given Face Impedances," *Sov. Phys. Dokl.*, Engl. Transl., 3, 752-755, 1958.

[19] J. L. Volakis and T. B. A. Senior,"Simple expressions for a function occurring in diffraction theory," *IEEE Trans. Antennas Propag.*, vol. AP-33, pp. 678-680, June 1985.

[20] J.L. Volakis and H.H. Syed, "Application of higher order boundary conditions to scattering by multilayer coated cylinders," *J. Electromag. Waves Applics.*, 1991.

[21] H.H. Syed and J.L. Volakis, "Diffraction by coated cylinders using higher order impedance boundary conditions," submitted to *IEEE Trans. Antennas Propagat.*

[22] K. Barkeshli and J.L. Volakis, "TE scattering by a two- dimensional groove in a ground plane using higher order boundary conditions," *IEEE Trans. Antennas Propagat.*, Oct. 1990.

Publications Resulting from this Research

Reports written (to date) related to this task

1. J.L. Volakis, T.B.A. Senior and J.M. Jin, "Derivation and Application of a Class of Generalized Impedance Boundary Conditions - II," University of Michigan Radiation Laboratory Technical Report 025921-1-T, February 1989. 38pp.

2. M.A. Ricoy and J.L. Volakis, "Derivation of Generalized Transition/ Boundary Conditions for the Planar Multiple Layer Structures," University of Michigan Radiation Laboratory, Technical Report 025921-5-T, August 1989. 36pp.

3. H.H. Syed and J.L. Volakis, "An Approximate Skew Incidence Diffraction Coefficient for an Impedance Wedge," University of Michigan Radiation Laboratory Report 025921-4-T.

4. M.A. Ricoy and J.L. Volakis, "Diffraction by a Multilayered Slab Recessed in a Ground Plane via the Generalized Impedance Boundary Conditions," University of Michigan Radiation Laboratory Report 025921-8-T.

5. H.H. Syed and J.L. Volakis, "An Asymptotic Analysis of the Plane Wave Scattering by a Smooth Impedance Cylinder," University of Michigan Radiation Laboratory Report 025921-9-T.

6. M.A. Ricoy and J.L. Volakis, "Electromagnetic Scattering from Two-Dimensional Thick Material Junctions," University of Michigan Radiation Laboratory Report 025921-14-T.

Papers written (to date) related to this task

1. T.B.A Senior and J.L. Volakis, "Derivation and Application of a Class of Generalized Impedance Boundary Conditions," *IEEE Trans. Antennas and Propagat.*, Vol. AP-37, pp. 1566-1572, December 1989.

2. M.A. Ricoy and J.L. Volakis, "Derivation of Generalized Transition/ Boundary Conditions from Planar Multiple Layer Structures," accepted in *Radio Science.*

3. J.L. Volakis and T.B.A. Senior, "Application of a Class of Generalized Boundary Conditions to Scattering by a Metal-Backed Dielectric Half-Plane," *Proceedings of the IEEE*, Vol. 77, No. 5, pp. 796-805, May 1989.

4. H.H. Syed and J.L. Volakis, "An Approximate Skew Incidence Diffraction Coefficient for an Impedance Wedge," submitted to *IEEE Trans. Antennas and Propagat.*

5. M.A. Ricoy and J.L. Volakis, "Diffraction by a Multilayered Slab Recessed in a Ground Plane via the Generalized Impedance Boundary Conditions," submitted to *Radio Science.*

6. M.A. Ricoy and J.L. Volakis, "Diffraction by a Symmetric Material Slab; Part I: General Solution," submitted to *IEEE Trans. Antennas and Propagat.*

7. M.A. Ricoy and J.L. Volakis, "Diffraction by a Symmetric Material Slab; Part II: Resolution of Non-Uniqueness Associated with Higher Order Boundary Conditions," submitted to *IEEE Trans. Antennas and Propagat.*

8. T.B.A. Senior and J.L. Volakis, "Generalized Impedance Boundary Conditions in Scattering," submitted to *Proceedings of the IEEE.*

Conference Papers/Presentations to date related to this task

1. J.L. Volakis and T.B.A. Senior, "Application of a Class of Generalized Boundary Conditions to Scattering by a Metal-Backed Dielectric Half Plane," 1988 Journess International De Nice Sur Les Antennas (JINA), Nice, France; Digest pp. 115-119.

2. J.L. Volakis and T.B.A. Senior, "Generalized Impedance Boundary Conditions for Dielectric Surfaces and Layers," 1989 National Radio Science Meeting, Boulder, CO, Session B-7, January 1989. Digest p. 211.

3. M.A. Ricoy and J.L. Volakis, "Derivation of Generalized Transition/ Boundary Conditions for Planar Multiple Layer Structures," 1990 National Radio Science Meeting, Boulder, CO.

4. H.H. Syed and J.L. Volakis, "An Approximate Diffraction Coefficient for an Impedance Wedge at Skew Incidence," 1989 IEEE AP-S/URSI Symposium, Session 57, San Jose, CA. AP-S Digest pp. 1286-1289.

5. M.A. Ricoy and J.L. Volakis, "Application of Higher Order Boundary Conditions in Scattering by Material Discontinuities," 1989 IEEE AP-S/URSI Symposium, Session 63, San Jose, CA. URSI Digest p. 279.

6. M.A. Ricoy and J.L. Volakis, "Application of Generalized Impedance Boundary Conditions to Diffraction by a Multilayered Metal-Dielectric Junctions," presented at the 1990 IEEE AP-S/URSI Symposium, Dallas, TX, URSI Digest p. 62.

7. H.H. Syed and J.L. Volakis, "Diffraction by a Smooth Coated Cylinder Simulated with Generalized Impedance Boundary Conditions," presented at the 1990 IEEE AP-S/URSI Symposium, Dallas, TX, URSI Digest p. 176.

8. J.L. Volakis and H.H. Syed, "Application of Higher Order Boundary Conditions to Scattering by Multilayered Coated Cylinders," 1990 IEEE AP-S/URSI Symposium, Dallas, TX, AP-S Digest pp. 586-589.

9. M.A. Ricoy and J.L. Volakis, "On the Analytical Implementation of Generalized Impedance Boundary Conditions," to be presented at the 1990 URSI General Assembly, Session B5, Prague, Chechoslovakia.

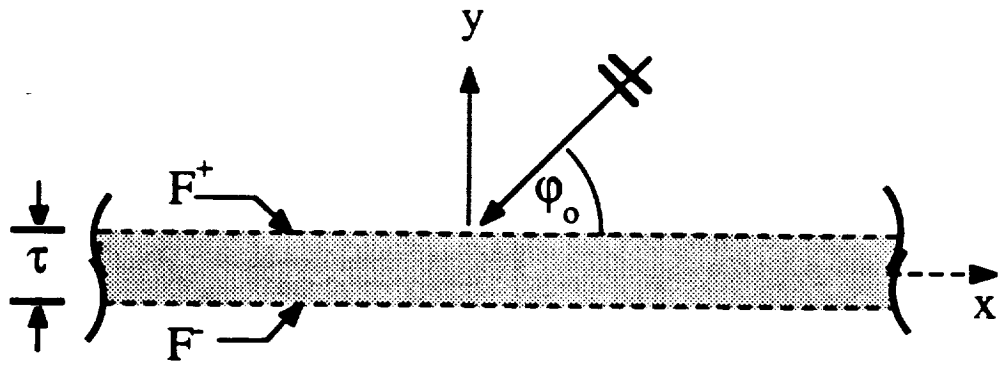

Odd GSTC: $u_{11}\left(-\frac{\partial x^2}{k^2}\right)\{F^+ - F^-\} + \frac{j}{k}u_{12}\left(-\frac{\partial x^2}{k^2}\right)\partial y\{F^+ + F^-\} = 0$

Even GSTC: $u_{21}\left(-\frac{\partial x^2}{k^2}\right)\{F^+ + F^-\} + \frac{j}{k}u_{22}\left(-\frac{\partial x^2}{k^2}\right)\partial y\{F^+ - F^-\} = 0$

(a)

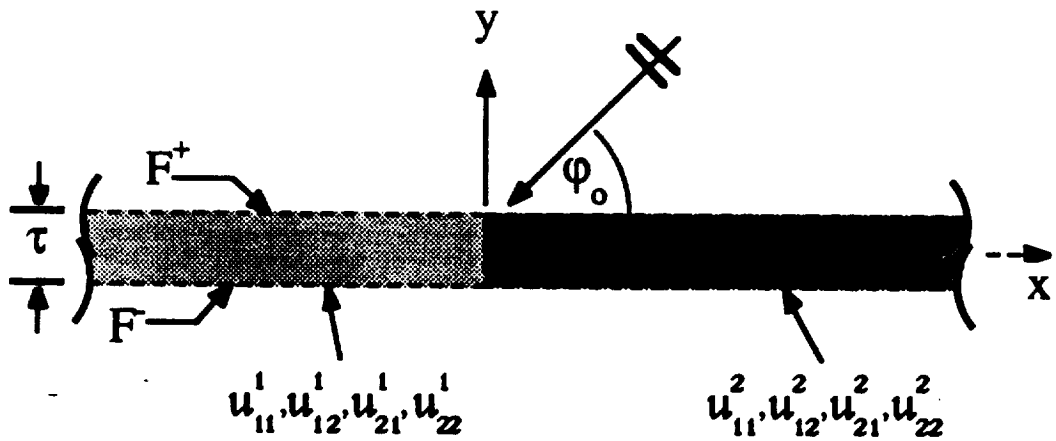

(b)

Figure 1. (a) Distributed sheet. (b) Distributed sheet discontinuity.

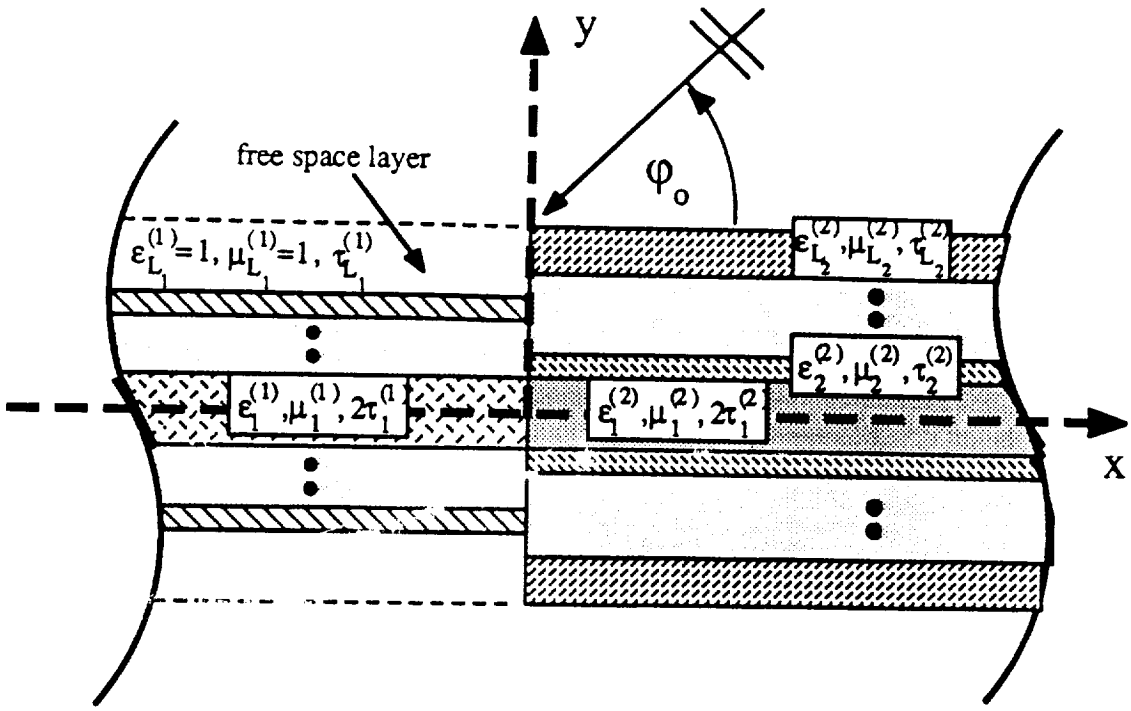

Figure 2. Geometry of the material-material join.

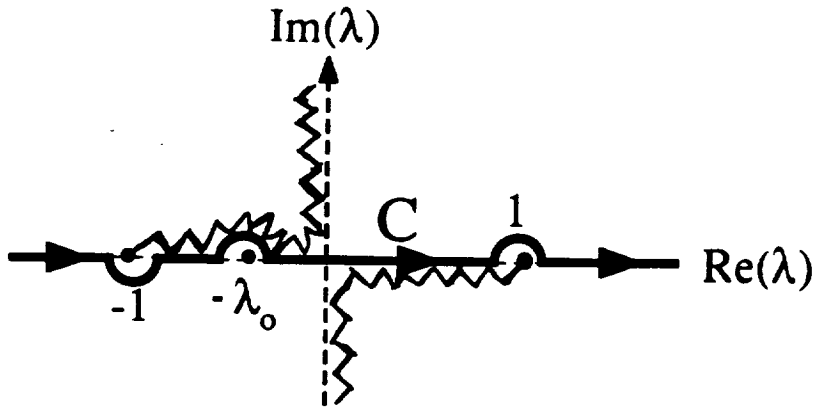

Figure 3. Illustration of the C contour in the complex λ-plane.

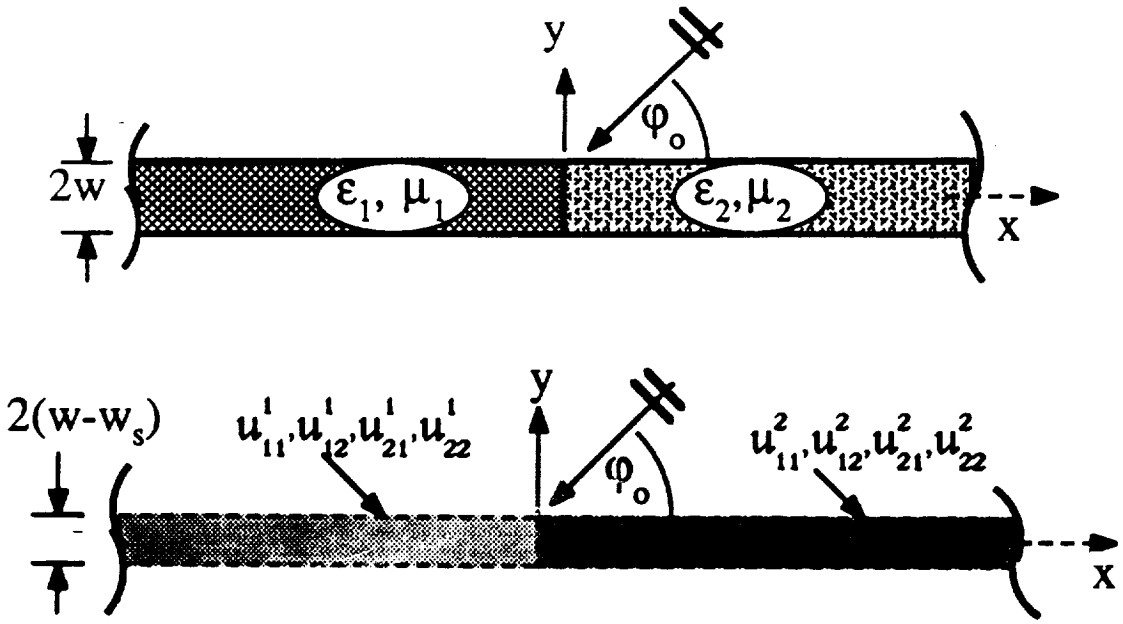

Figure 4. Thin discontinuous slab and its associated sheet representation.

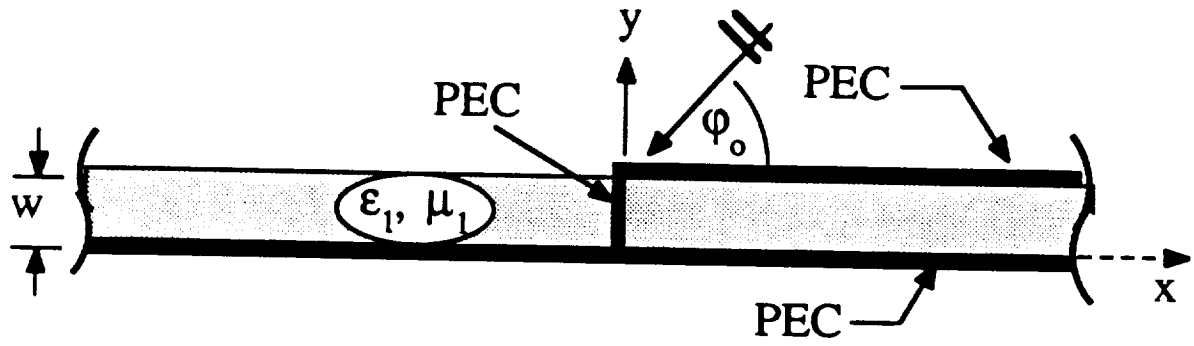

Figure 5. Recessed slab (PEC stub) on a ground plane.

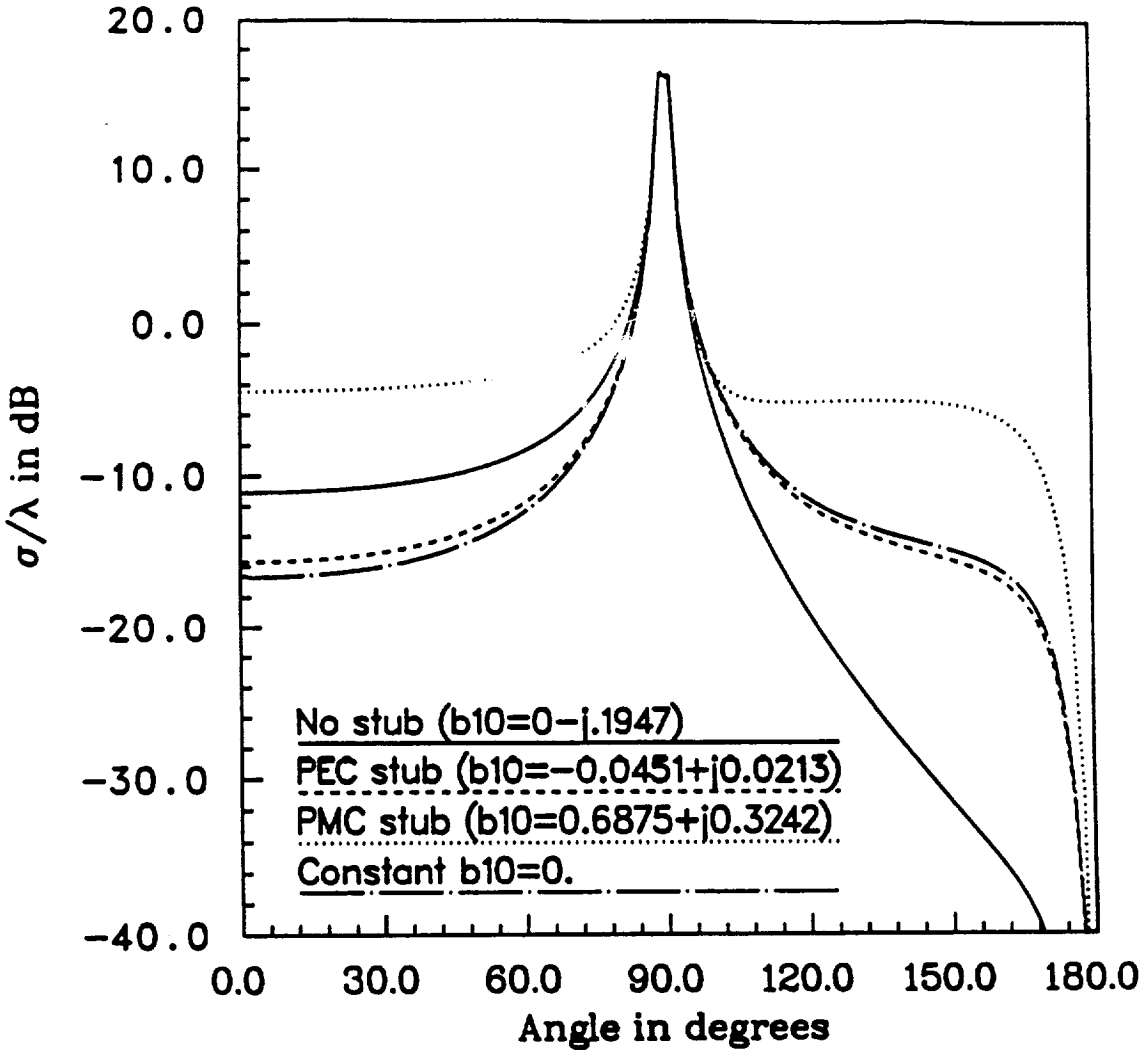

Figure 6. H_z-polarization backscatter echowidth for a material insert having w=0.04λ, ε=2-j.0001, μ=1.2 modeled with O(w) low contrast GIBCs.

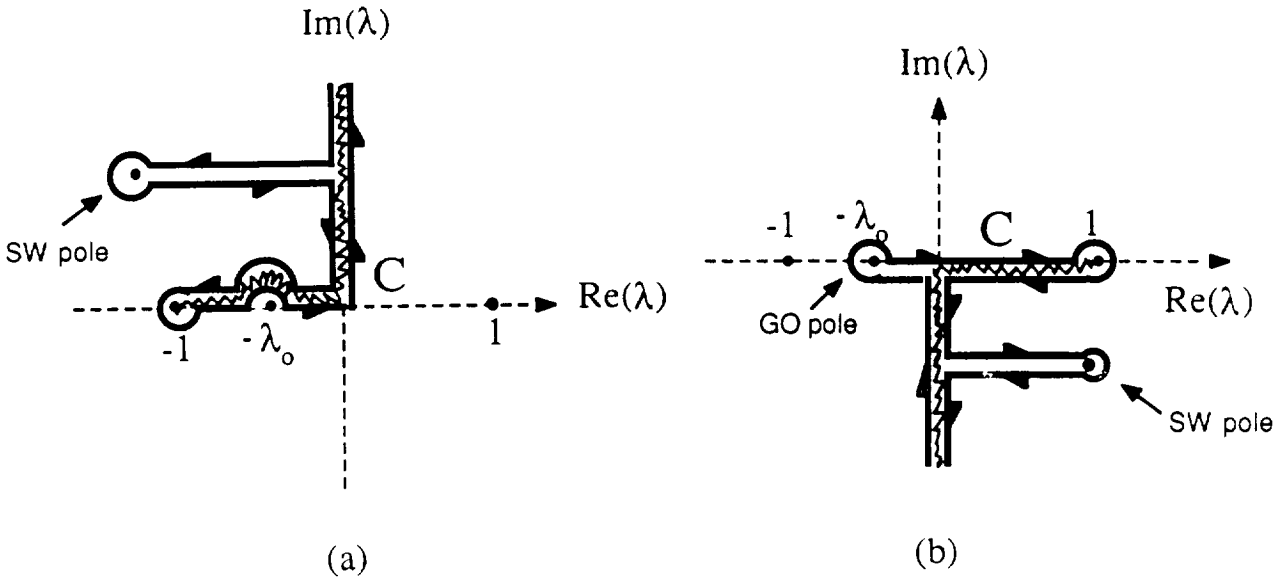

Figure 7. Deformation of the C contour for (a) region 1 integrals and (b) region 2 integrals.

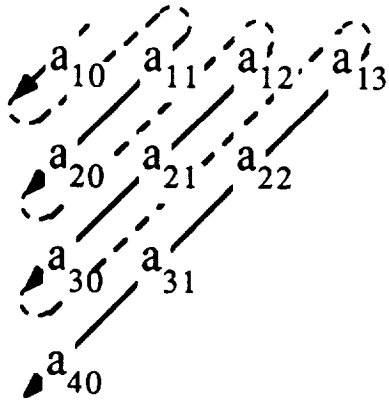

Figure 8. Indexing scheme for the constants.

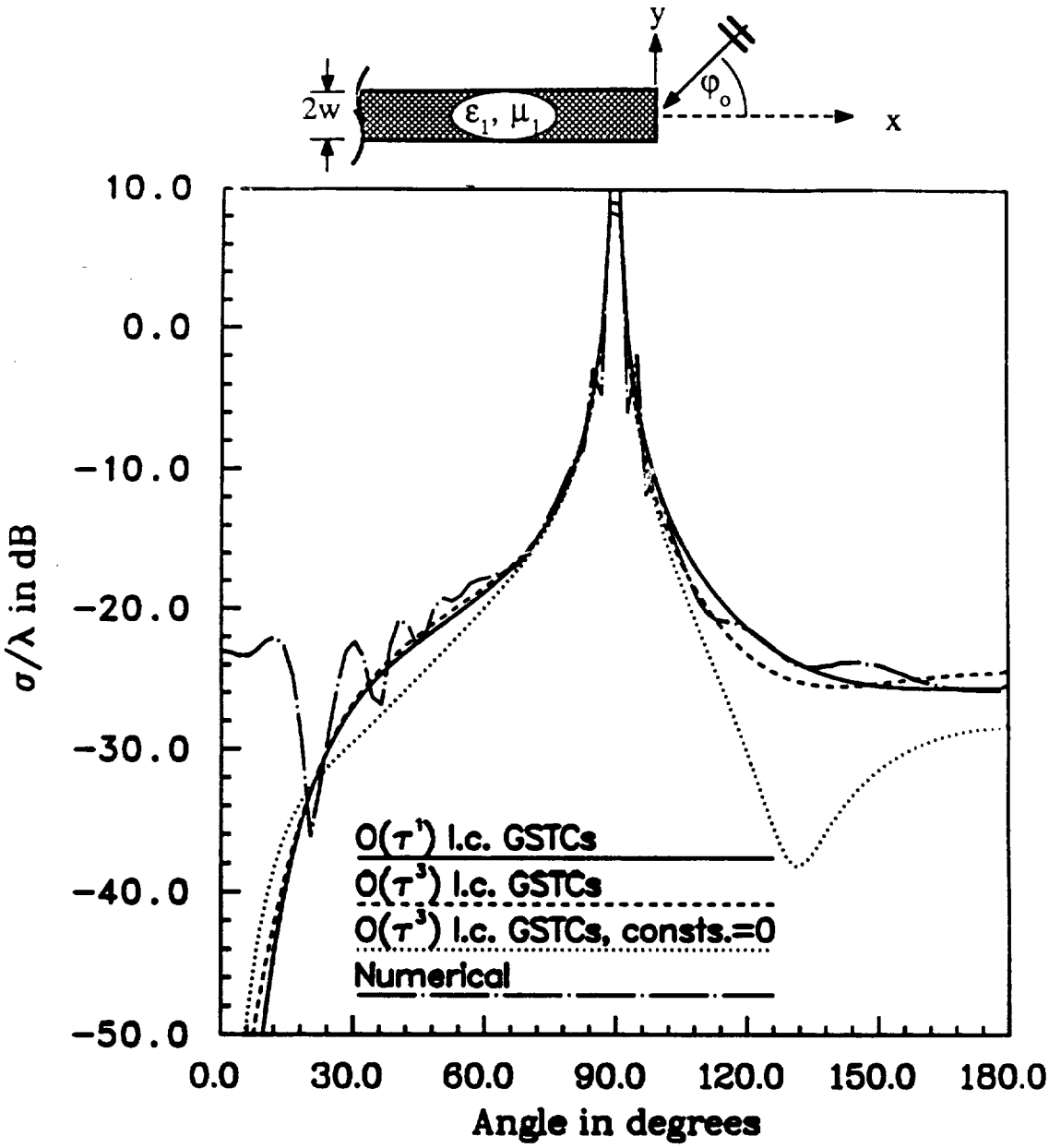

Figure 9. H_z-polarization backscatter echowidth for material half-plane with τ=.20, ε=2-j.0001, μ=1.2.

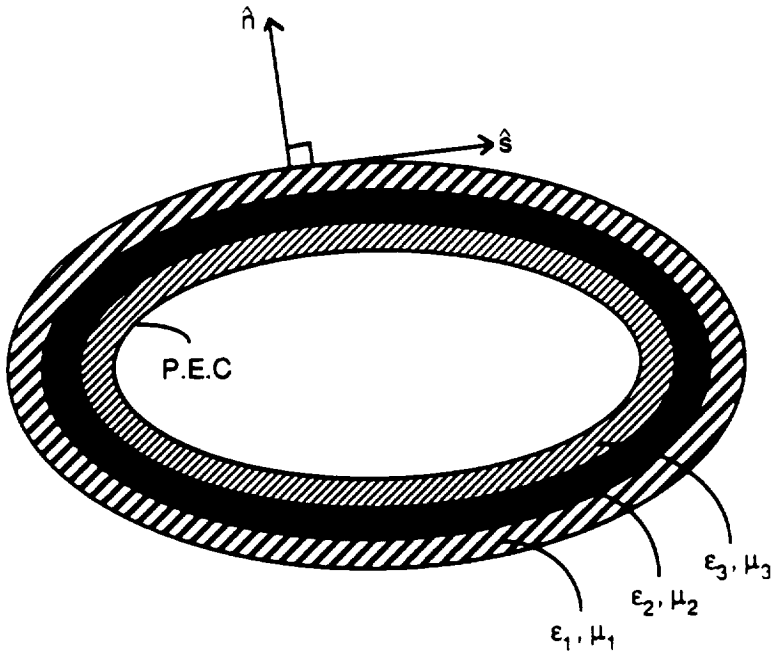

Figure 10. Illustration of a three-layer coated cylinder.

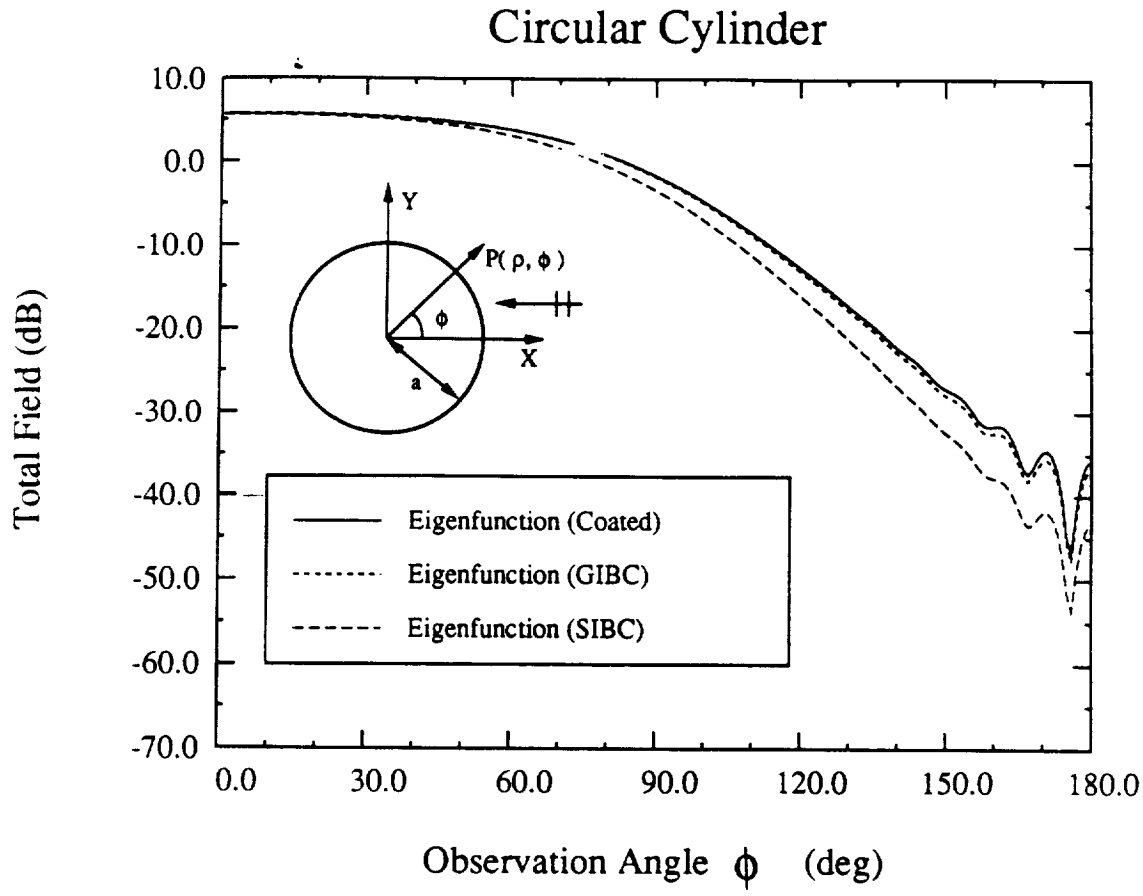

Figure 11. Bistatic H-polarization scattering pattern of a circular cylinder of Radius 2.93λ coated with a layer 0.07λ thick having ε=4 and μ=1; Comparison of fields at a distance 0.05λ away from the coatings surface.

Geometry, $x > 0$	$\mathcal{U}_{11}^2(-\cos\phi\cos\phi_o)$	$\mathcal{U}_{12}^2(-\cos\phi\cos\phi_o)$	$\mathcal{G}_{odd}^{2+}(\cos\phi)\,\mathcal{G}_{odd}^{2+}(\cos\phi_o)$	$\gamma^{odd,2}$
Low Contrast $O(w, w_s)$	1	$jk(u_2 w - w_s)$	$M_+\left(\cos\phi;\gamma_1^{odd,2}\right) M_+\left(\cos\phi_o;\gamma_1^{odd,2}\right)$	$\frac{-j}{k(u_2 w - w_s)}$
Free Space Limit	1	$jk(w - w_s)$	$M_+\left(\cos\phi;\gamma_1^{odd,2}\right) M_+\left(\cos\phi_o;\gamma_1^{odd,2}\right)$	$\frac{-j}{k(w - w_s)}$
PEC(Ez-pol) or PMC(Hz-pol)	1	0	1	———
PMC(Ez-pol) or PEC(Hz-pol)	0	1	$\sqrt{1-\cos\phi}\sqrt{1-\cos\phi_o}$	———

Table 1: Odd symmetry parameters associated with the right hand side material $x > 0$. See Appendix for the definition of the M_+ split functions.

Geometry, $x > 0$	$\mathcal{U}_{21}^2(-\cos\phi\cos\phi_o)$, $\mathcal{U}_{22}^2(-\cos\phi\cos\phi_o)$	$\mathcal{G}_{even}^{2+}(\cos\phi)\,\mathcal{G}_{even}^{2+}(\cos\phi_o)$
Low Contrast, $O(w, w_s)$	$\mathcal{U}_{21}^2 = jk\left(\frac{w\epsilon_2\mu_2}{u_2} - w_s\right)$ $+jk\cos\phi\cos\phi_o\left(\frac{w}{u_2} - w_s\right)$ $\mathcal{U}_{22}^2 = 1$	$\frac{jkw}{u_2}(\epsilon_2\mu_2 - 1)\prod_{m=1}^{2} M_+(\cos\phi;\gamma_m^{even,2}) M_+(\cos\phi_o;\gamma_m^{even,2})$ with $\gamma_{1,2}^{even,2} = \frac{u_2 \pm \sqrt{u_2^2 + 4k^2 w(\epsilon_2\mu_2 - 1)(w - u_2 w_s)}}{2jk(w - w_s u_2)}$
Free Space Limit	$\mathcal{U}_{21}^2 = jk(w - w_s)(1 + \cos\phi\cos\phi_o)$ $\mathcal{U}_{22}^2 = 1$	$\sqrt{1-\cos\phi}\sqrt{1-\cos\phi_o} M_+\left(\cos\phi;\gamma_1^{even,2}\right) M_+\left(\cos\phi_o;\gamma_1^{even,2}\right)$ with $\gamma_1^{even,2} = \frac{-j}{k(w - w_s)}$
PEC(Ez-pol) ($b_{10} = 0$) or PMC(Hz-pol) ($b_{10} = 0$)	$\mathcal{U}_{21}^2 = 1$ $\mathcal{U}_{22}^2 = 0$	1
PMC(Ez-pol) or PEC(Hz-pol)	$\mathcal{U}_{21}^2 = 0$ $\mathcal{U}_{22}^2 = 1$	$\sqrt{1-\cos\phi}\sqrt{1-\cos\phi_o}$

Table 2: Even symmetry parameters associated with the right hand side material $x > 0$. See Appendix for the definition of the M_+ split functions.